Towards IASI-New Generation (IASI-NG): impact of improved spectral resolution and radiometric noise on the retrieval of thermodynamic, chemistry and climate variables

Cyril Crevoisier, Cathy Clerbaux, Vincent Guidard, Thierry Phulpin, Raymond Armante, Blandine Barret, Claude Camy-Peyret, Jean-Pierre Chaboureau, Pierre-François Coheur, Laurent Crépeau, et al.

Atmos. Meas. Tech., 7, 4367–4385, 2014
www.atmos-meas-tech.net/7/4367/2014/
doi:10.5194/amt-7-4367-2014

Atmospheric Measurement Techniques
Open Access

Towards IASI-New Generation (IASI-NG): impact of improved spectral resolution and radiometric noise on the retrieval of thermodynamic, chemistry and climate variables

C. Crevoisier[1], C. Clerbaux[2], V. Guidard[3], T. Phulpin[4], R. Armante[1], B. Barret[5], C. Camy-Peyret[6], J.-P. Chaboureau[5], P.-F. Coheur[7], L. Crépeau[1], G. Dufour[8], L. Labonnote[9], L. Lavanant[10], J. Hadji-Lazaro[2], H. Herbin[9], N. Jacquinet-Husson[11], S. Payan[2], E. Péquignot[4], C. Pierangelo[4], P. Sellitto[8,*], and C. Stubenrauch[1]

[1]Laboratoire de Météorologie Dynamique, IPSL, CNRS, Ecole Polytechnique, Palaiseau, France
[2]UPMC Université Paris 6; Université Versailles St-Quentin; CNRS-INSU, LATMOS-IPSL, Paris, France
[3]Météo-France and CNRS / CNRM-GAME, Toulouse, France
[4]Centre National d'Etudes Spatiales (CNES), Toulouse, France
[5]Laboratoire d'Aérologie/OMP, University of Toulouse and CNRS, Toulouse, France
[6]Institut Pierre Simon Laplace, Paris, France
[7]Spectroscopie de l'Atmosphère, Service de Chimie Quantique et Photophysique, Université Libre de Bruxelles (ULB), Brussels, Belgium
[8]Laboratoire Interuniversitaire des Systèmes Atmosphériques, CNRS, Universités Paris Est Créteil et Paris Diderot, Créteil, France
[9]Laboratoire d'Optique Atmosphérique (LOA), Université Lille-1, Villeneuve d'Ascq, France
[10]Météo-France / CMS, Lannion, France
[11]Laboratoire de Météorologie Dynamique, IPSL, CNRS, UPMC Université Paris 6, Paris, France
[*]now at: Laboratoire de Météorologie Dynamique, IPSL, CNRS, Ecole Normale Supérieure, Paris, France

Correspondence to: C. Crevoisier (cyril.crevoisier@lmd.polytechnique.fr)

Received: 29 October 2013 – Published in Atmos. Meas. Tech. Discuss.: 19 December 2013
Revised: 29 September 2014 – Accepted: 7 October 2014 – Published: 10 December 2014

Abstract. Besides their strong contribution to weather forecast improvement through data assimilation, thermal infrared sounders onboard polar-orbiting platforms are now playing a key role for monitoring atmospheric composition changes. The Infrared Atmospheric Sounding Interferometer (IASI) instrument developed by the French space agency (CNES) and launched by EUMETSAT onboard the Metop satellite series is providing essential inputs for weather forecasting and pollution/climate monitoring owing to its smart combination of large horizontal swath, good spectral resolution and high radiometric performance. EUMETSAT is currently preparing the next polar-orbiting program (EPS-SG) with the Metop-SG satellite series that should be launched around 2020. In this framework, CNES is studying the concept of a new instrument, the IASI-New Generation (IASI-NG), characterized by an improvement of both spectral and radiometric characteristics as compared to IASI, with three objectives: (i) continuity of the IASI/Metop series; (ii) improvement of vertical resolution; and (iii) improvement of the accuracy and detection threshold for atmospheric and surface components. In this paper, we show that an improvement of spectral resolution and radiometric noise fulfil these objectives by leading to (i) a better vertical coverage in the lower part of the troposphere, thanks to the increase in spectral resolution; and (ii) an increase in the accuracy of the retrieval of several thermodynamic, climate and chemistry variables, thanks to the improved signal-to-noise ratio as well as less interference between the signatures of the absorbing species in the measured radiances. The detection limit of several atmospheric species is also improved. We conclude that IASI-NG has the potential to strongly benefit the numerical weather prediction,

chemistry and climate communities now connected through the European GMES/Copernicus initiative.

1 Introduction

Infrared sounders are a key element of space observation of the Earth system. They enable the monitoring of several thermodynamic, chemistry and climate variables over land and sea, night and day. In particular, the Infrared Atmospheric Sounding Interferometer (IASI) (Chalon et al., 2001), flying onboard Metop-A since October 2006 and Metop-B since September 2012, has demonstrated the possibility to retrieve or detect several chemistry and climate variables from hyperspectral infrared observation: for instance water vapour (H_2O), carbon dioxide (CO_2), carbon monoxide (CO), methane (CH_4), ozone (O_3), sulfur dioxide (SO_2), hydrogen sulfide (H_2S), ammonia (NH_3), nitric acid (HNO_3), volatile organic compounds (VOCs) and aerosols (Hilton et al., 2012; Clarisse et al., 2011) on regional and global scales. IASI has given access to species that had never previously been observed from space on a global scale (Clarisse et al., 2009; Razavi et al., 2011; Duflot et al., 2013) and enables the monitoring of key gases for climate and atmospheric chemistry in near real time. IASI has also highlighted the benefit of high-performance infrared sounders for numerical weather prevision (NWP) applications: IASI on Metop-A currently contributes more impact than any instrument on any satellite to the skill of the 24 h global forecast of several NWP centres (Météo-France, UK MetOffice, ECMWF) (Collard and McNally, 2009; Guidard et al., 2011, J. Eyre, personal communication, 2011).

Despite their good spatial and temporal coverage and their essential contribution to the three-dimensional characterization of the atmosphere, infrared sounders still suffer from a limited sensitivity to the lower part of the troposphere near the surface. For instance, with existing instruments, it is still challenging to identify temperature inversions or to retrieve with an adequate precision water vapour near the surface where it is the most abundant. Similarly, the measurement of the atmospheric concentration of short-lived species that are rapidly deposited or destroyed by chemical reactions in the atmosphere (e.g. NH_3, methanol) remains difficult since (i) their concentrations are highest near the surface; and (ii) their low abundance is such that their spectral signatures are usually hidden by the radiometric noise. One of the biggest challenges in chemistry and climate studies is thus the improvement of the characterization of the thermodynamic and atmospheric composition of the lower part of the troposphere. A better profiling of key atmospheric variables is also needed to improve NWP, to better understand boundary layer processes or to assimilate satellite-based retrievals in climate and air quality models. International programs, such as the World Climate Research Program (WCRP) or the Global Climate Observing System (GCOS), have thus stressed the need for improved atmospheric observations enabling a better characterization of the processes, the validation of models, and the long-term monitoring of atmospheric composition and climate (GCOS-107, 2006; GCOS-154, 2011).

As part of the Earth Polar System Second Generation (EPS-SG) program of the European Organisation for the Exploitation of Meteorological Satellites (EUMETSAT), the Centre National d'Etudes Spatiales (CNES) has initiated the study of the IASI-New Generation (IASI-NG) mission. Its main objectives are: (i) continuity of the IASI/Metop series; (ii) improvement of the vertical coverage and resolution, especially in the lower troposphere; and (iii) improvement of the precision and detection threshold of atmospheric and surface components. To fulfil these goals, IASI-NG will measure infrared radiation emitted by the Earth with improved spectral resolution and radiometric noise as compared to IASI. The spatial resolution of the instrument will be the same as for IASI (EUMETSAT, 2010), following the recommendation of the Post-EPS Mission Expert Team for answering the needs of NWP, chemistry and climate applications. In particular, the size of IASI-NG field of view will be the same as for IASI (about 12 km at nadir).

This paper presents results of the studies that have led to the definition of IASI-NG industrial specifications and focuses on how an improvement in either spectral resolution, radiometric characteristics or both can improve detection and retrieval of key atmospheric and surface variables. Section 2 presents the various scenarios and the methodology used to perform the studies. Section 3 focuses on the retrieval of thermodynamic variables atmospheric temperature and water vapour. Section 4 deals with other climate variables (CO_2, CH_4, surface characteristics). Section 5 focuses on the retrieval of trace gases (CO, O_3, other trace gases). Section 6 summarizes the expected performances of IASI-NG with regard to IASI.

2 Methodology to study the impact of spectral and radiometric characteristics

2.1 Spectral and radiometric scenarios

Similarly to IASI, IASI-NG will be a Fourier Transform Spectrometer that will measure infrared radiation emitted from the Earth. IASI-NG will provide 16923 (8461 for IASI) spectral samples, between 645.00 and 2760.00 cm^{-1} (15.5 and 3.63 µm), with a spectral resolution of 0.25 cm^{-1} (0.50 cm^{-1} for IASI) after apodization and a spectral sampling of 0.125 cm^{-1} (0.25 cm^{-1} for IASI). Apodized spectra are referred to as level-1c spectra.

Figure 1 shows the radiometric noise, in terms of level-1c noise-equivalent brightness temperature (NEΔT), expressed at a reference temperature T_{ref} of 280 K, spanning the spectral range 645–2760 cm^{-1} for different configurations: IASI actual noise (black line), IASI noise with a factor of 2 im-

Table 1. The six infrared sounder (IRS) scenarios.

Spectral resolution	IASI noise	IASI noise/2	IASI noise/4
IASI ($0.5\,\mathrm{cm}^{-1}$)	IRS1a (IASI)	IRS1b	IRS1c
IASI-NG ($0.25\,\mathrm{cm}^{-1}$)	IRS2a	IRS2b	IRS2c

provement (dark grey line), IASI noise with a factor of 4 improvement (light grey line), and the actual IASI-NG specifications (objective in blue and threshold in red) as specified by CNES. In the following sections, the radiometric noise for a given situation will be computed at the temperature of the scene BT(ν) for channel frequency ν, using the equation

$$\mathrm{Ne}\Delta T\left(\mathrm{BT}(\nu)\right) = \mathrm{Ne}\Delta T\left(T_{\mathrm{ref}},\nu\right) \times \frac{\partial B_\nu}{\partial T}\left(T_{\mathrm{ref}}\right) \Big/ \frac{\partial B_\nu}{\partial T}\left(\mathrm{BT}(\nu)\right), \quad (1)$$

where NEΔT is the equivalent noise temperature taken at the brightness temperature BT, of the channel frequency ν, and B is the radiance.

In the following, we will use six different scenarios, which are summarized in Table 1, to evaluate the impact of spectral and radiometric characteristics on the retrieval of various atmospheric and surface variables. The three scenarios IRS1a, IRS1b and IRS1c will assume a spectral resolution of $0.5\,\mathrm{cm}^{-1}$ (Gaussian apodization) and a noise corresponding to the current IASI noise, the IASI noise divided by 2 and the IASI noise divided by 4 respectively. These scenarios will help evaluate the improvement of the noise with regard to the IASI reference scenario (IRS1a). The three scenarios IRS2a, IRS2b and IRS2c will assume a spectral resolution of $0.25\,\mathrm{cm}^{-1}$ (Gaussian apodization) and the same three noise scenarios. As can be seen from Fig. 1, the IASI-NG objective and threshold radiometric noises (recommended upper and lower limit for noise specifications) pretty much cover the range of these scenarios.

2.2 Channel sensitivities to atmospheric and surface variables

Before performing the retrievals of atmospheric variables, the first step in evaluating the capability of an infrared sounder to retrieve these variables consists in identifying the spectral regions offering the optimal characteristics for the retrieval. Three criteria might be used: the target signal must be the highest possible, the target signal must be greater than the signals due to other variables (these will be called "interferences" in the following), and the channels must harmoniously cover the whole atmospheric column. To evaluate the impact of improved spectral resolution and radiometric noise on the two first criteria, we focus here on the sensitivity of the channels to major atmospheric and surface variables.

For a given atmospheric situation, the variation of the brightness temperature induced by a given variation of atmospheric and surface variables have been computed as

$$\Delta\mathrm{BT}\left(\nu,\Delta T\right) = \sum_{j=1}^{\mathrm{nl}} \frac{\partial \mathrm{BT}}{\partial T}\left(\nu,j\right) \times \Delta T\left(j\right) \quad (2)$$

for temperature and

$$\Delta\mathrm{BT}\left(\nu,\Delta q_{\mathrm{gas}}\right) = \sum_{j=1}^{\mathrm{nl}} \frac{\partial \mathrm{BT}}{\partial q_{\mathrm{gas}}}\left(\nu,j\right) \times \Delta q_{\mathrm{gas}}\left(j\right) \quad (3)$$

for a gas, where $\frac{\partial \mathrm{BT}}{\partial T}(\nu,j)$ and $\frac{\partial \mathrm{BT}}{\partial q_{\mathrm{gas}}}(\nu,j)$ are respectively the temperature and gas Jacobians at pressure layer j and nl is the number of pressure layers.

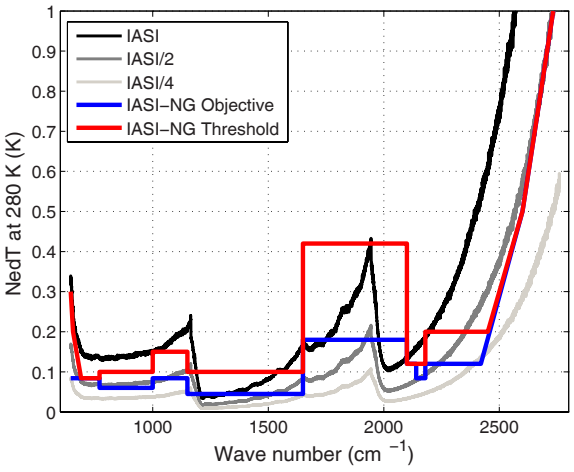

Figure 1. Radiometric noise expressed as level1c equivalent noise temperature NeΔT for a reference temperature of 280 K. The black line gives the in-flight measured IASI noise. Grey lines give the IASI noise when divided by a factor of 2 and 4. The current noise specifications for IASI-NG are plotted in red (threshold specification) and in blue (objective specification).

Figure 2 displays the channel sensitivity for the spectral resolution of IASI (IRS1a,b,c scenarios) and IASI-NG (IRS2a,b,c scenarios) to typical variations of the major atmospheric and surface variables, averaged over the whole representative tropical situations of the TIGR database (Chédin et al., 1985; Chevallier et al., 1998) (available at: http://ara.abct.lmd.polytechnique.fr/index.php?page=tigr): variations of 1 K for atmospheric and surface temperatures, 20 % for H_2O, 10 % for O_3, 1 % for CO_2, 10 % for CH_4, 10 % for CO, 2 % for N_2O, and 0.05 for surface emissivity (ε_s). The sensitivities computed over the whole temperate and polar situations of the TIGR database are plotted in the Supplement (Figs. S1 and S2). For a given channel, a negative sensitivity for a gas indicates that an increase of the gas concentration induces a colder BT, and thus a channel mostly sensitive to tropospheric variation of the gas concentration. Conversely, a positive sensitivity indicates a channel mostly sensitive to the stratosphere.

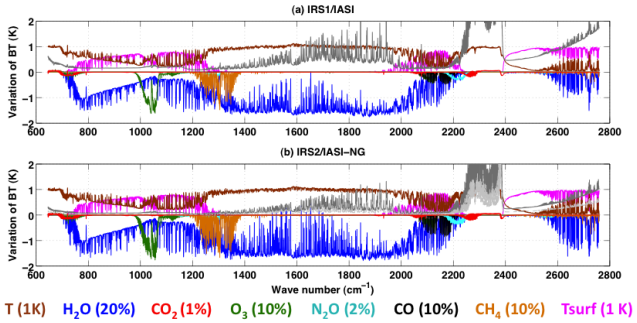

Figure 2. Sensitivities of infrared channels at the spectral resolution of IRS1/IASI **(a)** and IRS2/IASI-NG **(b)** to various atmospheric and surface variables and averaged over the whole tropical TIGR atmospheric situations. Variations of 1 K of temperature (brown), 20 % of water vapour (blue), 1 % of CO_2 (red), 10 % of O_3 (green), 2 % of N_2O (cyan), 10 % of CO (black), 10 % of CH_4 (orange) and 1 K of surface temperature (pink). Also shown is the radiometric noise of each scenario computed at the BT of the channels (grey): IASI noise in **(a)** and IASI noise divided by 2 (dark grey in **b**) and by 4 (light grey in **b**). The computation of channels sensitivities is based on simulations performed using the forward radiative transfer model 4A/OP (Scott and Chédin, 1981; http://4aop.noveltis.com/) based on the GEISA09 spectroscopic database (Jacquinet-Husson et al., 2011).

Figure 2 highlights the dominant role played by temperature and water vapour in the thermal infrared spectral range. The absorption bands of the other gases are also well seen in Fig. 2. They will be discussed in the following sections. The signatures of each variable given by the variation of BT can be compared to the radiometric noise computed at the BT of the scene according to Eq. (1) (grey line in Fig. 2). It is already apparent that the reduction of noise will particularly matter for gases having very small signature, whereas for other species, it will be more the improvement of spectral resolution that will matter in order to isolate the signature of each gas in the measured radiances.

To complement the study of the channels' sensitivities, which inform on the overall sensitivity of a given channel to variations of atmospheric variables along the whole atmospheric column, it is necessary to study the distribution of the sensitivity along the vertical which is given by the Jacobians. Two criteria will be used in the following: the mid-height width of the Jacobians, which must be the lowest possible, and the altitude of the maximum of the Jacobians.

2.3 Impact assessment

In the following, specific studies are undertaken to study the impact of the improvement of both the spectral and radiometric specifications on the vertical sensitivity and on the error associated with the retrieved variables. We use the IASI specifications as a baseline and the scenarios listed in Table 1 as the input variables for radiative transfer simulations.

The retrieval from space observation of a vertically resolved atmospheric profile is ill-conditioned, meaning that it has no unique solution. A likely solution can be obtained by regularizing the retrieval with a priori information about the variables. To study the impact of improved spectral resolution and radiometric noise on the retrieval, we rely on two retrieval techniques currently used to process IASI observations: the Optimal Estimation Method (OEM), and a non-linear inference scheme based on neural networks. They are briefly detailed below.

To study the scenarios, only nadir observations are considered. Experience with IASI has shown that retrieval performances are almost not affected by the angle of observation. Clear-sky conditions will also be assumed. Errors from radiative transfer modelling, spectroscopy, cloud residuals, or calibration will not be taken into account. The positive impact of a given improved scenario compared to the reference scenario will thus likely be overestimated. To circumvent these difficulties, it is not the absolute values of the errors that will be considered but their values for one scenario relative to another.

2.3.1 The optimal estimation method

In the optimal estimation method, which is described in detail by Rodgers (2000), the a priori information consists of a mean prior state and an a priori covariance matrix $\mathbf{S}_a$, which represent the best statistical knowledge that we have of the state prior to any measurement is made. The goal of the retrieval is then to find the approximation of the true state of the atmosphere that agrees best with both the measurements and the a priori information.

The characterization of the retrieved quantities in terms of vertical sensitivity and error sources is essential to determine the quality of the results. In the case of the linear approximation used here, the OEM provides an efficient way for characterizing the retrieved state. Two quantities will particularly be used in the following: (1) the Degrees Of Freedom for Signal (DOFs); (2) the total error variance–covariance matrix, which gives the a posteriori uncertainty. DOFs indicate the number of independent values of the state vector that can be retrieved from the measurements. They are given by the trace of the averaging kernel matrix $\mathbf{A}$, which is representative of the sensitivity of the retrieved state to the true state. The total error variance–covariance matrix $\mathbf{S}_e$ can be expressed as the sum of three individual contributions, according to

$$\mathbf{S}_e = (\mathbf{I}-\mathbf{A})\,\mathbf{S}_a(\mathbf{I}-\mathbf{A})^T + \mathbf{G}\mathbf{S}_\varepsilon\mathbf{G}^T + \mathbf{S}_{\text{model}}, \quad (4)$$

where $\mathbf{I}$ is the identity matrix and $\mathbf{G}$ is the gain matrix whose rows are the derivatives of the retrieved state with respect to the spectral points and which is related to $\mathbf{A}$ and to the Jacobian matrix $\mathbf{K}$ by

$$\mathbf{A} = \mathbf{G}\mathbf{K}. \quad (5)$$

The first term of Eq. (4) is the smoothing error, which accounts for the vertical sensitivity of the measurements to the retrieved profile and is related to the a priori covariance matrix $\mathbf{S}_a$. The second term is the measurement error, associated with the radiometric noise described by its covariance matrix $\mathbf{S}_\varepsilon$. The third term represents the imperfect knowledge of the model parameters. In the following, $\mathbf{S}_\varepsilon$ will be assumed diagonal, with the diagonal terms given by the square of the radiometric noise computed at the scene temperature given by Eq. (3). $\mathbf{S}_{\text{model}}$ has been chosen diagonal with a standard deviation of 0.2 K. This representation of forward model noise is not realistic, both in terms of value and inter-channel correlation, and attention needs to be paid to improving our knowledge of this error. Nevertheless, this value has been widely used in previous publications (Rodgers, 1996; Prunet et al., 1998; Crevoisier et al., 2003), and does not impact the values of the gain in uncertainty and vertical coverage reported here, since results are presented relative to each other.

2.3.2 Non-linear inference scheme

To avoid the linearization of the radiative transfer equation and to deal with signal of the order or lower than the radiometric noise, neural networks provide a powerful tool that is currently used to interpret IASI observations in terms of several trace gases. Here, we will use a non-linear inference scheme using supervised multi-layer perceptrons (Rumelhart et al., 1986) with two hidden layers. The learning phase, which consists in adapting the synoptic weights of the networks in order to minimize the output error using known input–output couples (the "a priori"), is based on the Error Back-Propagation learning algorithm (Rumelhart et al., 1986), with stochastic steepest descent. At each step of the learning phase, the instrument noise is taken into account by adding to the BT of each channel a random Gaussian noise characterized by the equivalent noise temperature (NEΔT) computed at the BT of the channel, according to Eq. (1). In this study, the learning database is the TIGR data set.

3 Impact on the retrieval of thermodynamic variables

Post-launch validation of retrievals of temperature and water vapour profiles derived from IASI has confirmed an accuracy of less than 1 K for temperature between 800 hPa and the tropopause and better than 10 % for relative humidity in the 800–300 hPa altitude range (Pougatchev et al., 2009; Kwon et al., 2012). However, as for any existing thermal infrared sounder, IASI still suffers from a limited sensitivity to the lower part of the troposphere near the surface, and to the tropopause region. Accordingly, the estimated accuracy reaches 2–3 K at the surface and ~ 2 K at the tropopause for temperature, and is higher than 10 % near the surface for H_2O where it is the most abundant. Improving the retrievals near the surface is thus a clear priority and one of the main objectives of the IASI-NG mission. It is worth noting that, beyond the impact on operational meteorology, any improvement in the characterization of the thermodynamic profiles will positively impact the retrievals of other atmospheric variables which usually require a good knowledge of the thermodynamic state of the atmosphere.

3.1 Atmospheric temperature

3.1.1 Sensitivity of IASI and IASI-NG channels to atmospheric temperature

Various spectral bands may be used to retrieve atmospheric temperature profiles. Those sensitive to stable components with low variability are preferred to ease the decorrelation between the temperature signature and the interferences in the infrared radiances. The most commonly used regions are the absorption bands of CO_2 around 667 cm^{-1} (15 µm) and around 2350 cm^{-1} (4.3 µm), even if, for IASI, the latter band is scarcely used due to the higher radiometric noise encountered there, as seen in Fig. 3.

In the 660–720 cm^{-1} region, the typical variation of BT temperature for a 1 K variation of atmospheric temperature (hereafter called the temperature signal) is between 0.6 and 1 K (Fig. 3a, c). From 660 to 690 cm^{-1} and from 704 to 720 cm^{-1}, line-mixing limits the use of channels located in the Q branch of CO_2. Recent work on line-mixing modelling (e.g. Niro et al., 2004a, b) opens the way to using this part of the spectrum. These cold regions would therefore strongly benefit from a reduction of the radiometric noise, which is still high for IASI (~ 0.4 K). Beyond 690 cm^{-1}, the range covered by the temperature signal is higher for the IRS2 (~ 0.3 K) than the IRS1 (~ 0.15 K) scenarios. This stems directly from the higher spectral resolution of IRS2 which induces an extended vertical resolution as explained below. For wavenumbers lower than 720 cm^{-1}, variations of BT induced by typical variations of other atmospheric variables are weak, generally lower than 0.15 K, with the exception of some channels located near 706 cm^{-1} and between 712 and 718 cm^{-1} which become sensitive to H_2O (variation of ~ 0.5 K of the BT for a 20 % variation of H_2O). Nonetheless, as opposed to IASI, it is possible to find IASI-NG channels for which temperature is decorrelated from H_2O and O_3. They are characterized by a null sensitivity to H_2O (blue line) and O_3 (green line) in Fig. 3c illustrating the capability of IASI-NG to resolve the most intense absorption lines of these two gases in this region.

In the 2200–2260 cm^{-1} region, the temperature signal varies between 0.5 and 1 K, with channels also sensitive to various atmospheric and surface components (Fig. 3b, d). The two most promising spectral ranges for temperature retrievals are 2200–2220 and 2230–2260 cm^{-1}, with a temperature signal of ~ 0.8 K and sensitivities to CO_2 and N_2O lower than 0.3 K. Due to their stability, CO_2 and N_2O are both suitable candidates for temperature retrieval (Lezeaux

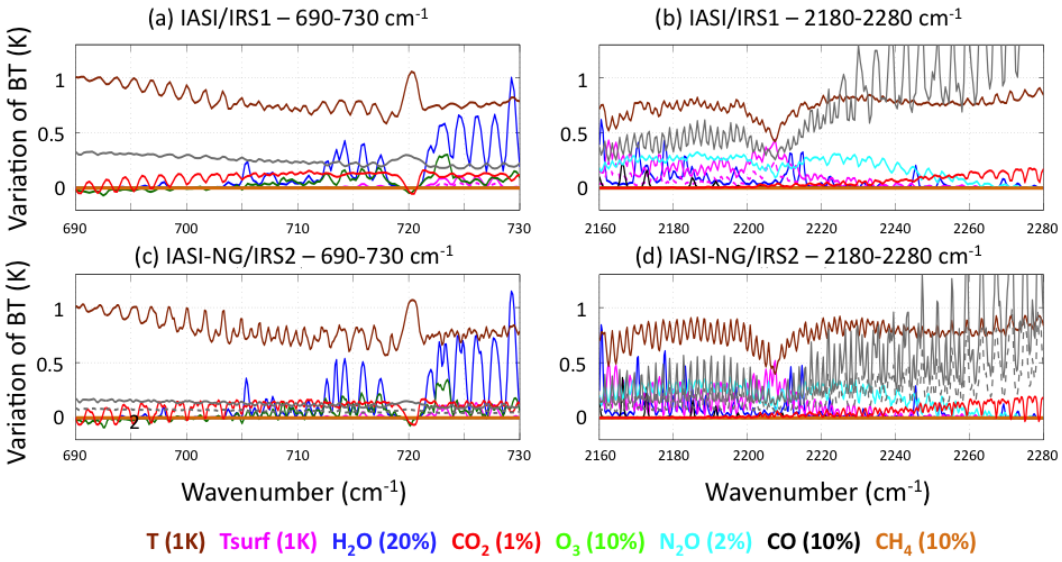

Figure 3. As Fig. 2, for the two spectral bands 690–730 and 2180–2280 cm^{-1}. To ease the comparison between the various signals, a factor of −1 has been applied to variations of BT for all the gases.

et al., 2010). As seen in Fig. 2, N_2O has two bands, one centred at 1258.6 cm^{-1} (ν_2), superpimposed with the ν_4 band of methane, and the ν_3 band at 2223.5 cm^{-1} superimposed with the end of the CO absorption band. However, N_2O natural variability is still poorly known and the corresponding channels should be handled with caution. Despite their good spectral characteristics, both spectral regions are characterized by a high noise on IASI (grey line in Fig. 3b), especially beyond 2230 cm^{-1}. Consequently, no IASI channels are currently used in this region to give information on atmospheric temperature. A strong reduction of the radiometric noise in this region will enable the use of the corresponding channels, which present the advantage of sounding the lower part of the atmosphere.

The mid-height width and altitude of the maximum of the temperature Jacobians are plotted in Fig. 4 for both IRS1 and IRS2 spectral resolutions. In the two regions of interest, the temperature Jacobians peak at all pressure levels. However, because of the higher spectral resolution of IRS2, the corresponding Jacobians peak at more levels than for IRS1 and are better distributed along the vertical. In particular, more channels peak at high altitudes, albeit with a larger width.

For instance, IRS2 Jacobians peak between 500 and 1000 hPa when IRS1 Jacobians "only" peak between 700 and 1000 hPa. Moreover, more channels covering the lower part of the troposphere are available with the IRS2 than with the IRS1 spectral resolution, and they are generally characterized by thinner Jacobians (half-height width between 300 and 400 hPa). This is also the case for channels located in the 2230–2260 cm^{-1} range, for which IRS1 Jacobians peak between 700 and 300 hPa whereas IRS2 Jacobians peak between 800 and 100 hPa. The widest IRS2 Jacobians (half-height width of about 700 hPa) peak at high altitudes that are not covered by IRS1-IASI.

3.1.2 Impact of spectral and radiometric characteristics on the retrieval of temperature profiles

To evaluate the expected retrieval accuracy and vertical coverage of each scenario given in Table 1, we use the optimal estimation method described in Sect. 2.3.1 in the general framework of NWP applications. The a priori covariance matrices $\mathbf{S}_a$ in Eq. (4) are from the ECMWF centre (Hólm et al., 2002). The a priori errors are already relatively low since they come from the assimilation of observations from several spaceborne instruments, radio-soundings, and surface networks. Improving them thus remains quite challenging. However, the resulting errors depend on the chosen a priori. Therefore, it is not their absolute values that should be considered but their values from one scenario relative to another. It must also be kept in mind that the error reduction brought by a given instrument is overestimated since these values are based on the use of all channels, and errors from radiative transfer modelling, cloud residuals or calibration are not taken into account.

First, only the band 645–770 cm^{-1} (all channels) is used in the retrieval procedure. As said in Sect. 3.1.1, the Jacobians of the corresponding channels do not peak at the surface. Therefore no information on the surface will be brought by this band alone. The number of degrees of freedom for each scenario is given in Table 2. The greater the spectral resolution and the lower the noise, the higher the number of DOFs. The number of DOFs for IASI (IRS1a) is low, highlighting the good a priori knowledge on temperature stemming from the assimilation of several observations. The better perfor-

Table 2. Number of degrees of freedom for the retrieval of temperature profile for the eight scenarios, using all the channels located in the 645–770 cm^{-1} range, or a combination of both the 645–770 and the 2250–2420 cm^{-1} ranges.

	IRS1a	IRS1b	IRS1c	IRS2a	IRS2b	IRS2c
645–770 cm^{-1}	3.2	5.6	7.1	4.4	7.7	9.8
645–770 and 2250–2420 cm^{-1}	3.3	5.8	7.3	4.6	8.0	10.0

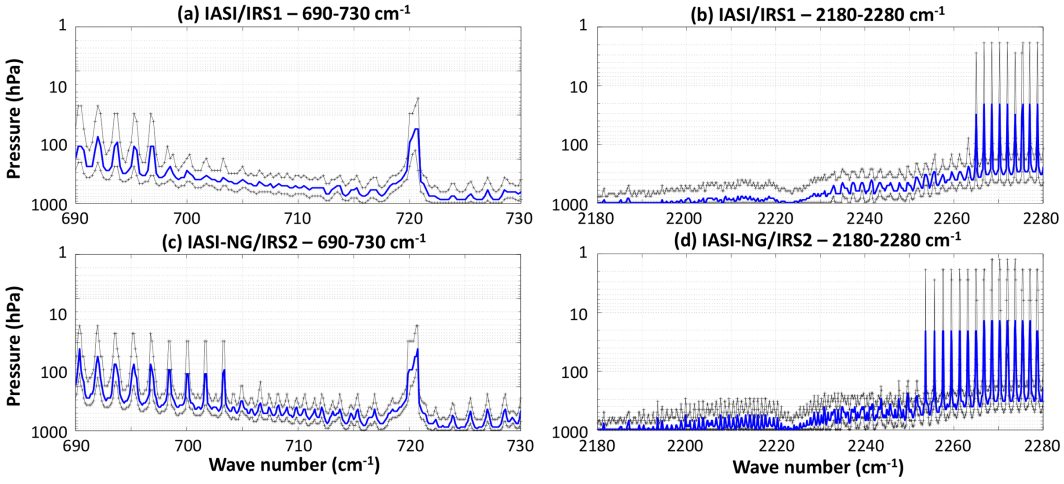

Figure 4. Pressure of the maximum (blue line) and of the half-height width (black) of the temperature Jacobians at the IASI spectral resolution in the 15 µm **(a)** and 4.3 µm **(b)** bands and at the IASI-NG spectral resolution in the 15 µm **(c)** and 4.3 µm **(d)** bands. The Jacobians have been computed by 4A and averaged over the whole tropical atmospheric situations of the TIGR database.

mance of the IRS2 scenarios as compared to IASI does not come only from the improved noise (IRS1b is worse than IRS2b), but neither from the greater resolution alone (IRS2b is similar to IRS1c). Taking into account the sole radiometric noise or also adding the uncertainties in water vapour and surface characteristics does not change this result.

The relative gain in retrieval uncertainty to the a priori is given by the difference between the a posteriori and the a priori errors, normalized by the a priori error. It is plotted in Fig. 5a. A factor of $\sim 1.5/2$ depending on the altitude is well seen between IRS1a-IASI (dashed blue line) and the IRS2a (full blue line) scenario. At 500 hPa, the gain is 20 % for IRS2a compared to 12 % for IRS1a-IASI. The comparison between IRS2a and IRS1b or IRS1c reveals that a greater spectral resolution brings a significant improvement in addition to the one stemming from the reduction of the radiometric noise. The strong reduction of the gain below 950 hPa comes from the fact that the retrieval of temperature profile is done independently from the retrieval of surface temperature, and reveals the lack of information brought by IR sounders in the lowest vertical layers apart from window channels informing of surface temperature.

Second, a combination of the whole channels located in the two bands 645–770 and 2250–2420 cm^{-1} is used. Both the number of DOFs and the relative gain are close even if better than when using the first band alone. The differ-

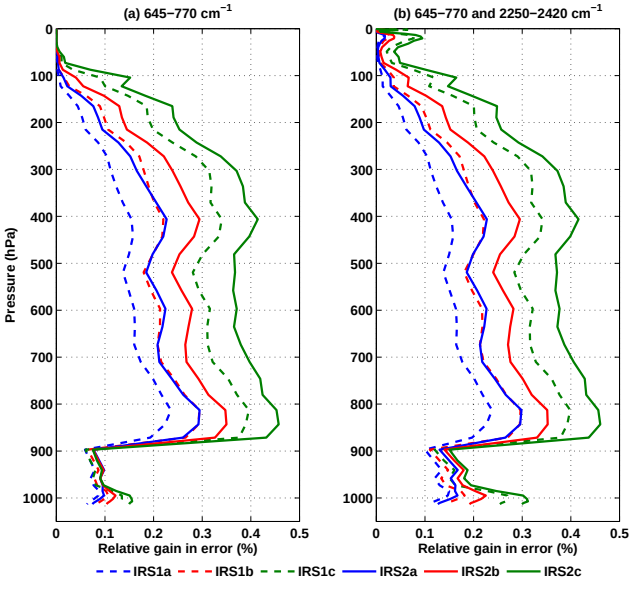

Figure 5. Impact of spectral resolution and radiometric noise on the retrieval of temperature profile based on the use of the 645–770 cm^{-1} spectral band **(a)** or of the 645–770 and 2250–2420 cm^{-1} spectral bands combined **(b)**. The relative gain in error is defined as the difference between the a priori and a posteriori error, divided by the a priori error, averaged over the whole tropical TIGR situations.

ence comes from the lower part of the troposphere as seen in Fig. 5b. Near the surface, the improvement is significantly better, as expected from the better coverage of this part of the atmospheric column by the temperature Jacobians (Fig. 4). Moreover, the reduction of the noise by a factor better than 2 (IRS1c and IRS2c) compared to IRS1a-IASI strongly improves the retrieval near the surface, highlighting that the reduction of the noise in that part of the spectrum is particularly relevant.

3.2 Water vapour

3.2.1 Sensitivity of IASI and IASI-NG channels to water vapour

As seen in Fig. 2, H_2O absorption lines span the entire spectral range covered by IASI, with the ν_2 absorption band extending from 1200 to 2150 cm^{-1}. Between 800 and 1200 cm^{-1}, the water vapour continuum is particularly important. The spectral range between 1400 and 2150 cm^{-1} is the most sensitive to water vapour variation (with a signal around 1.5 K for a variation of 20 % in Fig. 2). In the regions below 770 cm^{-1} and between 950 and 1050 cm^{-1} CO_2 and O_3 interfering absorption lines are found and the channel sensitivity to a 20 % variation of H_2O is lower than 0.5 K. Moreover, these lines are saturated and could potentially induce a bias or large uncertainties on retrieved quantities. Therefore, to retrieve atmospheric water vapour information from high-resolution thermal infrared measurements, many previous studies using various instruments such as IMG (Zakharov et al., 2004; Herbin et al., 2007), TES (Worden et al., 2006), or IASI (Herbin et al., 2009; Lacour et al., 2012) have restricted the retrieval spectral range to between 1100 and 1400 cm^{-1}.

Figure 6 represents the half-height widths and altitudes of the maximum of the H_2O Jacobians for the water vapour full absorption band. Within this spectral range, the Jacobians reach all pressure levels from 800 to 100 hPa (2 to 16 km). However, the maxima of water vapour Jacobians cover a wider range of pressure levels for the IRS2-IASI-NG scenarios thanks to their higher spectral resolution. They are also better distributed along the vertical. The number of channels with large Jacobian values at high altitudes is larger, particularly in the 1500–2150 cm^{-1} spectral band.

3.2.2 Impact of spectral and radiometric characteristics on the water vapour retrieval

Table 3 summarizes the total DOFs for all scenarios, when using all channels located in the 1100–1400 cm^{-1} band. The impact of reducing the radiometric noise is small on the DOFs when the improvement of the spectral resolution has a clear positive impact on the DOFs since the IRS2 scenarios all give better results than the IRS1c scenario.

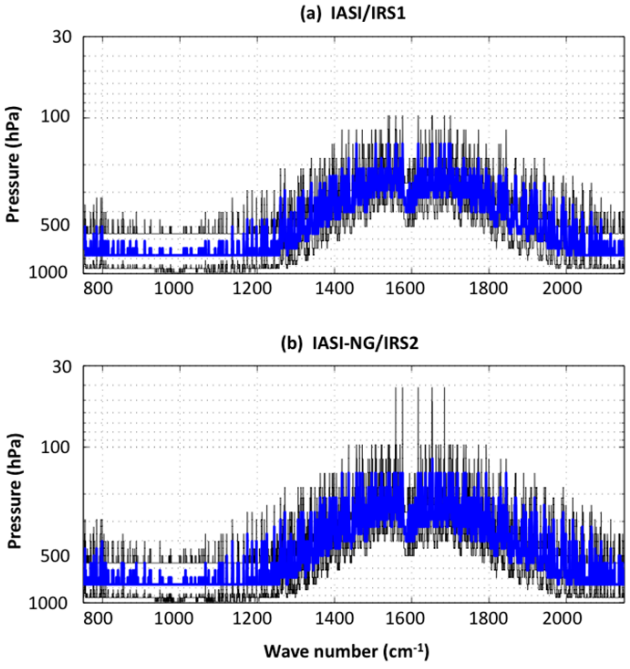

Figure 6. Pressure of the maximum (blue line) and of the half-height width (black) of the H_2O Jacobians at the IASI spectral resolution (upper panel) and at the IASI-NG spectral resolution (bottom panel). Average over the TIGR tropical atmospheric situations.

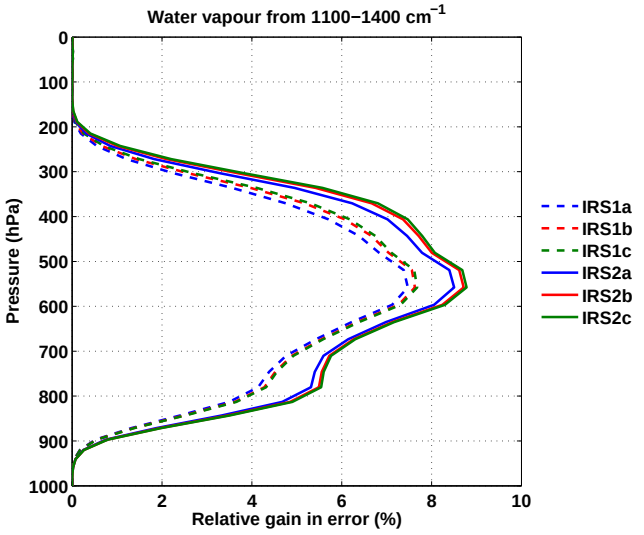

Figure 7. Impact of spectral resolution and radiometric noise on the retrieval of water vapour profile based on the use of the 1100–1400 cm^{-1} spectral band. The relative gain in error is defined as the difference between the a priori and a posteriori error, divided by the a priori error, averaged over the whole tropical TIGR situations.

Figure 7 shows the relative gain in error, defined as the difference between the a priori and a posteriori error divided by the a priori error, for each scenario, from which similar conclusions as from DOFs can be drawn. A much larger con-

Table 3. Number of degrees of freedom for the retrieval of water vapour profile for the six scenarios, using all channels located in the 1100–1400 cm^{-1} spectral range.

	IRS1a	IRS1b	IRS1c	IRS2a	IRS2b	IRS2c
1100–1400 cm^{-1}	11.7	11.8	11.8	14.5	14.5	14.6

tribution of the higher spectral resolution than the reduced noise is well seen: the gain in error is higher for the IRS2 scenarios, whatever the noise reduction is. The most significant gain is between 700 and 300 hPa (3 and 8 km). Above 300 hPa, the impact of noise and spectral resolution is limited and of the same order of magnitude.

4 Other climate variables

Since its launch onboard Metop-A in October 2006, IASI contributes to the establishment of robust long-term data records of several essential climate variables (ECVs) as defined by GCOS: (i) clouds: cloud physical properties using the atmospheric opacity of the CO_2 absorbing channels and cirrus bulk microphysical properties based on the spectral variation between 8 and 12 µm; (ii) greenhouse gases: mid-tropospheric columns of CO_2 and CH_4 (Crevoisier et al., 2009a, b, 2013); (iii) dust aerosols: aerosol optical depth, altitude and radius (Peyridieu et al., 2013; Klüser et al., 2012; Clarisse et al., 2010); (iv) continental surface characteristics: skin temperature and spectral emissivity (Capelle et al., 2012; Zhou et al., 2011). IASI has the potential to monitor the evolution of these variables in the long term, to assess potential trends, and to detect signatures of specific climate events, such as ENSO or other sources of climate variability. The IASI-NG instrument, by extending the temporal coverage of the IASI mission with a similar approach, will help in minimizing the risk of strong inter-instrument bias, thus complying to the GCOS principles. Assuming that IASI-NG will present the same outstanding spectral and radiometric stability as IASI, it will also strongly contribute to the GSICS (Global Space-based Inter-Calibration System, http://gsics.wmo.int) effort.

In the following sections, we focus on three ECVs: CO_2, CH_4 and surface characteristics. Despite the fact that infrared remote sensing provides a way to characterize clouds and aerosols, as well as the thermal part of their total radiative forcing, the study of the impact of improved spectral and radiometric characteristics on their retrieval requires extensive study of several types of particles in non-clear situations (i.e. taking diffusion into account), inducing heavy computation. This will thus be addressed in a following paper.

4.1 Carbon dioxide

4.1.1 Sensitivity of IASI and IASI-NG channels to CO_2

CO_2 has three absorption bands in the part of the spectrum covered by the instruments: the ν_2 band centred at 667.4 cm^{-1} (15 µm), the ν_3 band centred at 2349.2 cm^{-1} (4.3 µm), and the weakest laser band centred at 1064 cm^{-1} (9.4 µm). In the latter region, the channel sensitivity to CO_2 variations is very low and the interferences with other species (H_2O, O_3) are quite high, preventing the use of the corresponding channels in the retrieval of CO_2. In the two other regions, the CO_2 signature for a 1 % variation comes to 0.15 K at 15 µm and 0.2 K at 4.3 µm. In comparison, a 1 K variation of the atmospheric temperature yields a variation of BT between 0.7 and 0.9 K at 15 µm and 0.7 and 1 K at 4.3 µm. Any CO_2 retrieval thus requires the decorrelation between temperature and CO_2 signals. In order to make this possible, channels with the lowest sensitivity to other components must be found (Chédin et al., 2003; Crevoisier et al., 2003).

In the ν_2 absorption band, the use of the 640–690 cm^{-1} range requires taking into account the line-mixing effect (Q branches at 660 cm^{-1}). Moreover, channel sensitivities to CO_2 are particularly weak (less than 0.1 K) for both IASI and IASI-NG, and the channels are sensitive to stratospheric variations of CO_2. Hence, in the following, we will focus on the 690–730 cm^{-1} spectral range since, for wave numbers higher than 690 cm^{-1}, the better spectral resolution of IRS2 enables the selection of channels with lower sensitivities to ozone and water vapour. The vertical coverage of the channels is similar for both resolutions. However, channels presenting the highest sensitivities to CO_2 tend to present CO_2 Jacobians that are thinner and peaking lower for IRS2 than IRS1 scenarios. As for atmospheric temperature, more pressure levels are covered by IRS2. The Jacobians of the IRS2 channels presenting the lowest sensitivities to atmospheric variables other than CO_2 cover the pressure range 110–400 hPa (7–15 km), with an average mid-height width 210 hPa. Whatever the spectral resolution is, only information on CO_2 in the mid-to-upper troposphere is available with channels located at 15 µm.

The ν_3 absorption band at 4.3 µm complements well the ν_2 absorption band at 15 µm since it gives information on CO_2 in a lower part of the atmosphere, closer to the surface (Crevoisier et al., 2003). CO_2 Jacobians peak between 350 and 600 hPa (4–8 km), with an average mid-height width of 400 hPa. Unfortunately, in this band, IASI radiometric noise exceeds 3 K (more than 30 times the CO_2 signal), thus precluding the use of the corresponding channels to retrieve CO_2. Reducing the radiometric noise is this part of the spectrum is thus a clearly identified need that will also benefit the retrieval of atmospheric temperature (see Sect. 3.1).

Table 4. Impact of spectral resolution, radiometric noise on the accuracy of the retrieval of CO_2 tropospheric columns, expressed relative to the IRS1a/IASI accuracy (%). Three spectral ranges are used: either the 15 µm band, or the 4.3 µm band or both bands. Note that IRS1a/IASI and IRS2a CO_2 retrievals are only performed with the 15 µm band.

	IRS1b	IRS1c	IRS2a	IRS2b	IRS2c
15 µm	10	24	9	30	40
4.3 µm	–	5	–	−7	14
15 and 4.3 µm	–	41	–	45	54

4.1.2 Retrieval of CO_2 tropospheric columns

We now study the impact of spectral resolution and radiometric noise on the retrieval of CO_2 mid and upper tropospheric columns using the non-linear inference scheme developed for IASI (Crevoisier et al., 2009a) and briefly described in Sect. 2.3.2. Only a subset of channels is used for the retrievals, based on their high sensitivity to CO_2, with no sensitivity to other species. Since infrared CO_2-sensitive channels are intrinsically sensitive to temperature, use is made of simultaneous microwave measurements, only sensitive to temperature, to separate these two effects. Now, although a microwave sounder will be one of the companion instruments of IASI-NG onboard Metop-SG, its specifications have not yet been chosen. Therefore, in the following, we will assume that an AMSU instrument, similar to the one onboard Metop, will fly onboard Metop-SG. We will also assume that both microwave and infrared sounders are co-registered, as is the case with IASI and AMSU.

Table 4 gives the improvement in the relative retrieval error obtained for the various scenarios with regards to the current IASI instrument (with 15 µm channels only) as a reference. An important characteristic of the retrieval is the CO_2 weighting function that indicates which part of the atmosphere the retrievals are representative of (Crevoisier et al., 2009a). This is plotted in Fig. 8 for various scenarios.

As expected, the better the spectral resolution or the radiometric noise, the larger the improvement of the retrieval error when the same spectral range is used. At the IASI spectral resolution, and using only the 15 µm band, reducing the noise by a factor of 2 or 4 already improves the error by 10 and 24 %. With similar noise, the improvement for the IRS2 scenario is even larger – 30 and 40 % respectively. This can be attributed to the better spectral resolution, which enables the use of more channels with stronger CO_2 signatures and less interference, hence reinforcing the "signal-to-noise" ratio even more than by simply reducing the noise. When using the 15 µm band only, the CO_2 weighting functions are close: for both the IRS1 and IRS2 scenarios, the channels give access to a mid-to-upper tropospheric content of CO_2 (100–400 hPa), with a maximum sensitivity near 200 hPa (Fig. 8). Nonetheless, thanks to its greater spectral

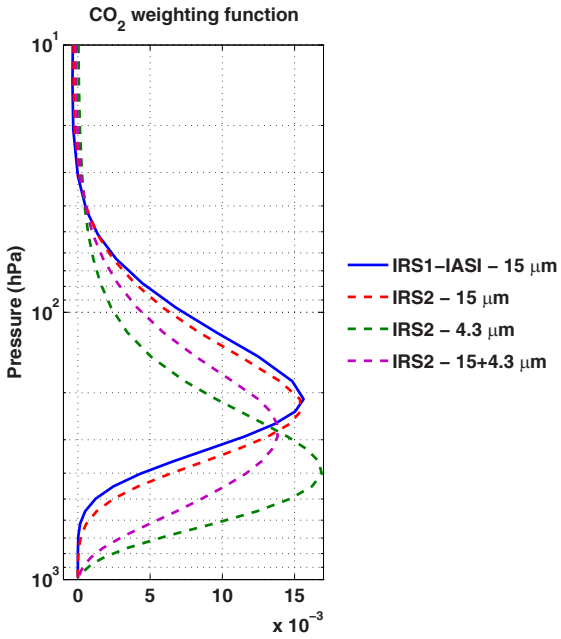

Figure 8. CO_2 weighting function associated with the retrieval for IRS1 scenarios using the channels located in the 15 µm CO_2 absorption band only (red) and for the IRS2 scenarios using the channels located either in the 15 µm CO_2 absorption band (blue), in the 4.3 µm CO_2 absorption band (dashed green), or in both bands (dot-dashed purple).

resolution, and in agreement with the study of the Jacobians performed in Sect. 3.1.1, the IRS2 CO_2 weighting function peaks at slightly lower altitudes than for IRS1.

When possible, the use of the sole 4.3 µm band gives access to a lower part of the atmosphere: the corresponding CO_2 weighting function peaks at 400 hPa (∼ 7 km) and covers the range 200—650 hPa (Fig. 8). Due to too large a radiometric noise compared to the CO_2 signal, the scenarios IRS1a-IASI, IRS1b and IRS2a do not offer this option. Compared to the retrieval error obtained for IRS1a-IASI using the 15 µm band, the error obtained for IRS2b with the 4.3 µm band is higher by 7 %; it is lower by 14 % for IRS2c when the noise is divided by a factor of 4. This is in agreement with the combination of a CO_2-to-noise ratio of the same order as the IRS1a-IASI one and a better spectral resolution. Therefore, with an increase by 2 of the spectral resolution, and a reduction by at least a factor of 2 of the radiometric noise, two pieces of information will be available for CO_2 along the vertical, both with improved retrieval errors compared to IASI.

In the case that the two spectral bands are used together, the retrieval error is divided by a factor of ∼ 2 compared to IRS1a-IASI, but at the expense of the vertical coverage. The CO_2 weighting function (Fig. 8) now covers a broad altitude range (100–500 hPa) with a maximum sensitivity near 300 hPa (∼ 9 km).

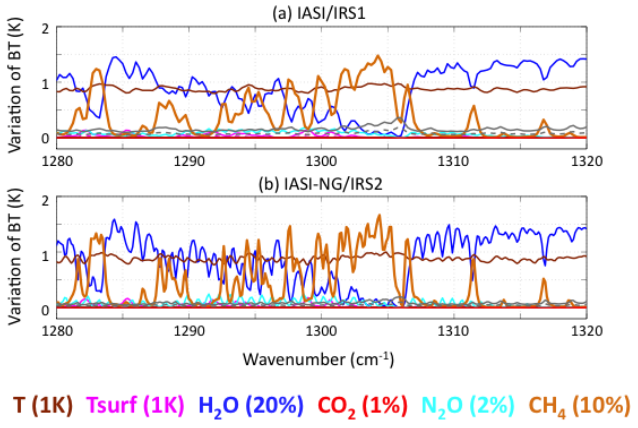

Figure 9. As Fig. 2, for the $CH_4 \nu_4$ absorption band.

4.2 Methane

4.2.1 Channel sensitivity to CH_4

Methane has two absorption bands in the part of the spectrum covered by the instruments: the ν_4 band centred at 1306.2 cm^{-1} ($\sim$ 7.7 µm) extending between 1220 and 1400 cm^{-1}, and the ν_3 band centred at 3020.3 cm^{-1} ($\sim$ 3.7 µm) which has lines at the far end of the spectra studied here, above 2680 cm^{-1}. In the ν_4 absorption band, water vapour absorption largely dominates, with mean sensitivities of 1 K for a 20 % variation of its mixing ratio (Fig. 9). The CH_4 signature for a 10 % variation of the gas mixing ratio is similar for IRS1 and IRS2 scenarios, even if a bit higher (0.2 K) for the latter, with values as high as 1.6 K. Here, having a better spectral resolution is a real asset since it allows finding spectral intervals where the CH_4 signal "comes out" of the H_2O signal: near 1300 cm^{-1}, as for IASI, but also near 1275 cm^{-1} (with a slight contamination by N_2O), 1247 cm^{-1} (with a slight contamination by the surface), or near 1340 cm^{-1}. In these regions, temperature signal is about 0.8 to 0.9 K, and the radiometric noise, which is much lower than the CH_4 signal, should not greatly impact the retrieval. The CH_4 Jacobians for these channels peak at 250 hPa and cover the range 150–500 hPa.

In the ν_3 absorption band at 3.3 µm, which gives access to channels sensitive to the lower troposphere, atmospheric and surface temperatures, emissivity and reflectivity have the major impact and dominate the CH_4 signal. Hence, the use of this band, which is also sensitive to solar radiation, requires a good knowledge of surface characteristics. Moreover, the CH_4 signal is much lower than the radiometric noise whatever the scenario is, except beyond 2700 cm^{-1} where it is lower by a factor of 2 to (of the same level as) the noise improved by a factor of 2 (resp. 4). Retrieving CH_4 atmospheric content from this part of the spectrum, which is also strongly sensitive to solar radiation, will thus remain very challenging and will only be possible in particular conditions. In the following, results are presented for the 7.7 µm band only.

Table 5. Impact of spectral resolution and radiometric noise on the accuracy of the retrieval of CH_4 tropospheric columns, expressed relative to the IRS1a-IASI accuracy (%).

	IRS1b	IRS1c	IRS2a	IRS2b	IRS2c
Gain (%)	5	9	39	44	47

4.2.2 Impact of spectral resolution and radiometric noise on the retrieval of CH_4

Using the non-linear inference scheme described in Sect. 2.3.2 and described in detail in Crevoisier et al. (2009b), we now study the impact of improving the spectral resolution and the radiometric noise on the retrieval of a CH_4 mid-tropospheric integrated content. The results are given in Table 5. Contrary to CO_2, reducing the radiometric noise does not impact much the retrieval error. This is because the IASI radiometric noise is already much lower than the CH_4 signal. On the other hand, by giving access to more channels with reduced sensitivity to water vapour, decreasing the spectral resolution improves the retrieval by decreasing the error by $\sim$ 40 %. The CH_4 weighting functions (not shown) are very similar whatever the scenario is with a maximum sensitivity near 250 hPa, with a covering range between 100–500 hPa.

4.3 Surface spectral emissivity

The MultiSpectral Method (MSM) currently used for retrieving mean surface skin temperature and emissivity spectra from 3.7 to 14 µm at a resolution of 0.05 µm from IASI (Péquignot et al., 2008; Capelle et al., 2012) was used to evaluate the expected performance of each scenario on the retrieval of spectral emissivity. As described in these papers, the standard deviation of the method is evaluated using a large set of synthetic simulations comprised of a randomly selected atmospheric situation from the TIGR database, an emissivity spectrum from a laboratory emissivity database and a surface temperature randomly selected within a realistic range.

Figure 10 displays the mean of the difference between the retrieved emissivity spectra and the reference ones averaged over the set of simulations for the IRS1a, b and c scenarios. For IRS1a-IASI, the standard deviation estimated for the spectral emissivity varies from about 0.01–0.015 % for the 10.5–14 and 5.5–8 µm windows to about 0.04–0.05 around 4 µm. The error is at its maximum in the two Reststrahlen bands, around 8–10 and 4 µm, because of (i) the higher emissivity variability; (ii) the higher impact of errors in the thermodynamic characterization of the atmosphere; and (iii) a higher radiometric noise (see Fig. 1). Therefore, reducing the noise helps in decreasing the error: as seen in Fig. 10, a re-

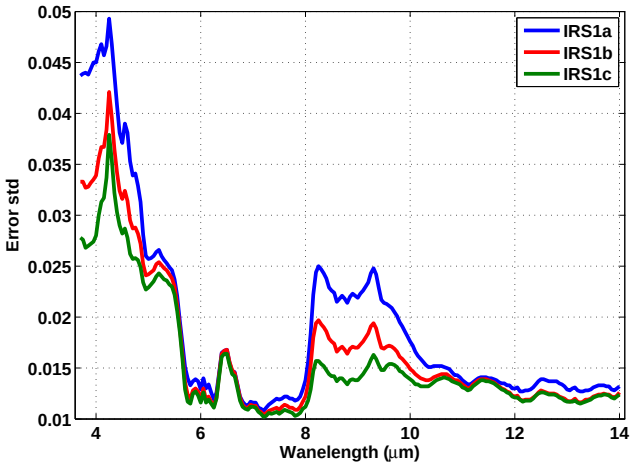

Figure 10. Impact of radiometric noise on the retrieval of surface spectral emissivity: standard deviation of retrieved emissivity for IRS1a-IASI (blue), IRS1b (red), IRS1c (green).

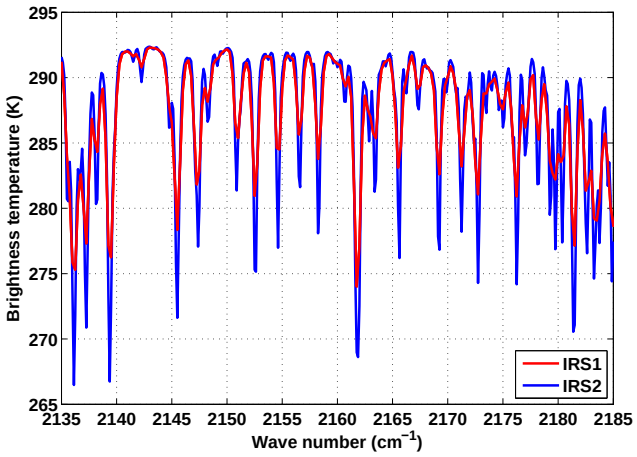

Figure 11. Impact of spectral resolution on the CO lines in the 2135–2185 cm^{-1} spectral range used for the CO retrieval – average over the whole tropical TIGR situations.

duction of the radiometric noise by a factor of 2 (4) decreases the error by 1.4 (1.6) at 12 μm and by 1.3 (1.7) at 4 μm. However, increasing the spectral resolution does not change the results since the channels used in the MSM method show similar characteristics for IRS1 or IRS2 scenarios.

5 Atmospheric chemistry

In this section, thermal infrared spectra are analysed for monitoring tropospheric composition and for the study of its rapid changes. Carbon monoxide, ozone, ammonia and sulfur dioxide are among the key products observed by the IASI mission (Clerbaux et al., 2009; Clarisse et al., 2009). Global and local distributions of trace gases are routinely derived using several inverse radiative transfer codes depending on the application (global maps, local profiles or detection of special events).

As described in the previous sections the different noise/spectral resolution scenarios for IASI-NG (see Table 1) are used to simulate IASI-NG like spectra in order to assess the potential improvement for trace gas retrieval or detection. For air pollution studies, improvement in terms of accuracy and also the ability to sound lower in the atmosphere are of particular interest. In the following, the retrieval procedure is based on the optimal estimation method described in Sect. 2.3.1 with error covariance matrices from Hurtmans et al. (2012): results for O_3 and CO are provided with DOFs as a metric to quantify the improvement in terms of vertical information, and retrieval errors are estimated for different layers of the atmosphere and reported relative to IRS1a-IASI.

5.1 Carbon monoxide

5.1.1 Sensitivity of IASI and IASI-NG channels to CO

The absorption band of carbon monoxide (CO) covers the range 2080 to 2200 cm^{-1}. CO absorbs the infrared radiation mainly in its 1–0 vibrational band, centred near 2140 cm^{-1} (Fig. 11). The spectral region has interferences with lines associated with H_2O, CO_2, N_2O, and O_3 absorption (Fig. 2). At the IASI0-IRS1 spectral resolution, all channels suffer from weak to medium contamination from these absorbing molecules. The CO content is retrieved using the 2143–2181.25 cm^{-1} spectral range, which offers the best compromise between information content and interferences with other gases (De Wachter et al., 2012). As can be seen from Fig. 11, by increasing the spectral resolution, the lines are better resolved, yielding an increased information content for CO. This is in agreement with results comparing the capability of AIRS and IASI instruments to retrieve CO (George et al., 2009; Thonat et al., 2012; Gambacorta et al., 2014).

5.1.2 Retrieval of CO

The CO tropospheric column is usually measured with 10 % accuracy or better from IASI, and with a maximum of two independent pieces of information on the vertical (George et al., 2009; Kerzenmacher et al., 2012). The sensitivity to the lower layers of the atmosphere is directly linked to thermal contrast, which is the difference between land surface skin temperature and surface-level air temperature and varies a lot according to season, latitude, time of the day and type of surface.

The simulations performed in this work using the different scenarios were done for a range of thermal contrasts, and for a series of representative atmospheric CO profiles.

Table 6. Improvement in terms of errors expressed in relative gain (%) from the IRS1a-IASI scenario for different atmospheric layers: CO total column, 6–12 km column, 0–6 km column and 0–2 km column.

	IRS1b	IRS1c	IRS2a	IRS2b	IRS2c
Total column	19	36	25	39	49
6–12 km	17	34	26	40	52
0–6 km	25	45	32	51	63
0–2 km	13	25	17	27	36

Table 7. Vertical information expressed in DOFs of the CO retrievals for each scenario.

	IRS1a	IRS1b	IRS1c	IRS2a	IRS2b	IRS2c
DOFs	1.84	2.20	2.6	2.28	2.65	2.98

The improvement of the error for different atmospheric layers (total column, 6 to 12, 0 to 6 and 0 to 2 km) is provided in Table 6. The improvement in terms of vertical information is provided in Table 7. As expected, both the improved spectral resolution and the better signal-to-noise lead to better resolved profiles: DOFs range from 1.8 for IRS1a-IASI to almost 3 for the best-case scenario (IRS2c), on average; as compared to IRS1a-IASI, reduction in total column error goes from 19 % for IRS1b to 49 % for IRS2c. The major improvement concerns the 0–6 km column with a major impact of spectral resolution: the reduction of the error is 32 % when improving the spectral resolution by a factor of 2 and keeping the noise at the same level (IRS2a) whereas it is only 25 % when the spectral resolution is kept and the noise is reduced by a factor of 2 (IRS1b). It should be noticed in particular that the boundary layer is better sounded, with a gain of 36 % for the IRS2c scenario. The error still remains more than 4 times higher than the error on the total column.

These results are confirmed when comparing CO profiles retrieved for scenarios IRS1a-IASI and IRS2b together with actual MOZAIC aircraft profiles measured at the Frankfurt airport in 2008 and 2009 that have already been used by De Wachter et al. (2012) for IASI-CO validation. In particular, comparisons have shown that IASI was enable to detect high CO concentrations in the wintertime/early-spring period when the boundary layer is low and polluted and the thermal contrast is low. Agreement between IASI and MOZAIC profiles was much better during late-spring/summer when CO concentrations are lower and the thermal contrast is higher. We have therefore selected two MOZAIC Frankfurt profiles representative of these contrasted conditions in order to highlight the differences between the six scenarios. As seen in Fig. 12, there is a significant impact near the surface, in particular for the less favourable polluted winter case (left): a value of 270 ppbv is retrieved at 1 km, which is close to the MOZAIC measured value of 265 ppbv, whereas the CO retrieved with the IRS1a scenario is too low, at 177 ppbv only (close to the a priori value of 130 ppbv), as observed with IASI. This is in agreement with a higher DOFs for IRS2b (2.4 for this case) than for IRS1a (1.9 for this case). However, due to the still limited vertical resolution, a positive bias is seen at 2–3 km for the IRS2b scenario. Even for the more favourable case of 26 May (Fig. 12, right), the IRS2b scenario gives much better results than the IRS1a scenario at all altitudes with DOFs reaching 3 and 2.3 respectively.

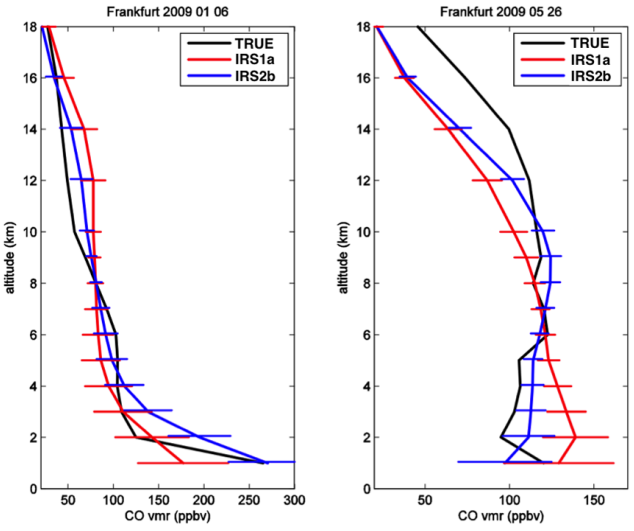

Figure 12. Impact of spectral resolution and radiometric noise on the CO retrieved profiles for cases IRS1a-IASI (red) and IRS2b (blue), compared with CO aircraft observation (in black). The left (right) plot corresponds to observation taken at Frankfurt airport on 6 January 2009 (26 May 2009).

5.2 Ozone

5.2.1 Sensitivity of IASI and IASI-NG channels to ozone

In the thermal infrared, ozone (O_3) has two absorption bands, the strongest one near 1042 cm^{-1} (ν_3 9.7 µm band) and a weaker one centred at 701 cm^{-1} (ν_2) where ozone signatures are mixed with those of H_2O and CO_2 (Fig. 2). The most prominent band extends from 980 to 1100 cm^{-1} (see Fig. 13). It is only slightly perturbed by other weak absorption features of H_2O and CO_2. Previous experience has demonstrated that the TIR measurements provide information on the ozone vertical profile from the ground up to an altitude of about 40 km, with a maximum sensitivity located in the mid-troposphere (Worden et al., 2007; Boynard et al., 2009; Dufour et al., 2012). The density of the spectra makes it difficult to discriminate individual lines and hence information in the boundary layer can hardly be obtained.

Table 8. Improvement in terms of errors expressed in relative gain (%) from the IRS1a-IASI scenario for different atmospheric layers: O_3 total column, 6–12 km column, 0–6 km column and 0–2 km column.

	IRS1b	IRS1c	IRS2a	IRS2b	IRS2c
Total column	25	39	21	39	51
6–12 km	9	17	7	18	31
0–6 km	9	19	7	20	35
0–2 km	4	10	3	11	21

Table 9. Vertical information expressed in DOFs of the ozone retrievals for each scenario.

	IRS1a	IRS1b	IRS1c	IRS2a	IRS2b	IRS2c
DOFs	3.59	4.10	4.65	3.97	4.70	5.45

5.2.2 Retrieval of ozone

Improvement in terms of errors and vertical information for the different scenarios and atmospheric scenarios are summarized in Tables 8 and 9. It is clearly seen that improving spectral resolution and radiometric noise improves the vertical sensitivity, and that most of the improvement in terms of accuracy is in the 0–6 km layer. In the lower atmosphere, between the surface and 2 km, there is only a limited improvement when the instrumental specifications are improved, except when both the signal/noise and spectral resolution are optimized (IRS2c). This is due to the fact that the ozone radiance channels are sensitive to several atmospheric layers and the density of the lines makes it hard to discriminate contributions from near the ground and above. On average, the DOF for IRS1a-IASI is around four pieces of independent information. It increases to five for the best-case scenario (IRS2c).

For air quality purposes, there is a need to discriminate tropospheric ozone from stratospheric ozone, which is a complicated task using a nadir thermal infrared sounder as there is a major absorption contribution due to high levels of stratospheric ozone encountered along the optical path. For most of the atmospheric situations, with the noticeable exception of high thermal contrast cases, tropospheric columns are associated with DOFs lower than one, which means that part of the information in the retrieved tropospheric product comes from the a priori information. In order to investigate how increasing the spectral resolution and reducing the radiometric noise helps to improve this situation, a variant of OEM, based on an altitude-dependent Tikhonov–Philips regularization matrix (Kulawik et al., 2006; Eremenko et al., 2008) instead of an a priori covariance matrix, has also been used (Sellitto et al., 2013). Simulations were done to evaluate the tropospheric ozone distributions as observed over Europe using a regional model, both for the IRS1a/IASI case and the improvement by a factor of 2 for spectral resolution and signal-to-noise ratio (IRS2b scenario). Figure 14 provides the DOFs (top) associated with the (0–6) km columns for a polluted case over Europe, as well as the maximum altitude (bottom) for the corresponding averaging kernel. It can be seen that the 0–6 km DOFs exceeds one for the IRS2b simulation, with associated maximum sensitivities lower in the atmosphere (2 to 4 km instead of 5 km or higher).

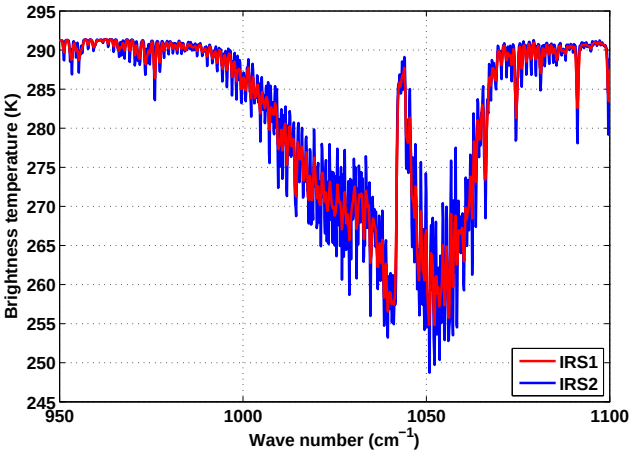

Figure 13. Impact of spectral resolution on the ozone lines in the 950–1100 cm^{-1} spectral range used for the ozone retrieval. Average over the whole tropical TIGR situations.

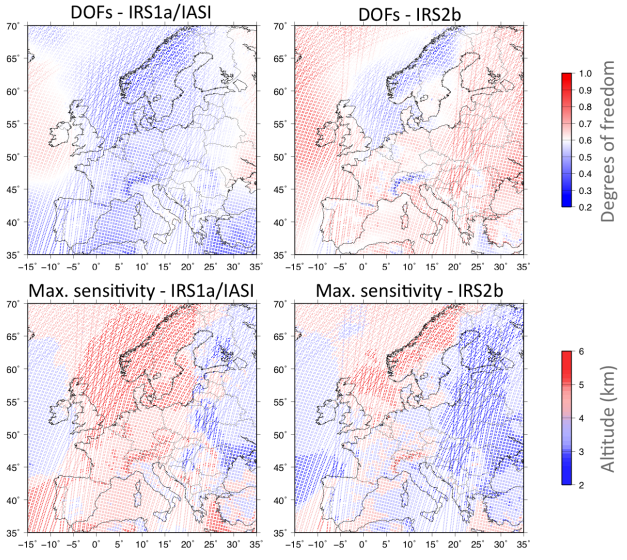

Figure 14. DOFs (top) and altitude of the maximum sensitivity (bottom, in kilometres) associated with the 0–6 km ozone retrieved on 20 August 2009, for IRS1a/IASI (left) and for the IRS2b scenario (right). This simulation was performed using a regional model that described an increase of ozone observed in Europe at that time. See Sellitto et al. (2013) for a full description of this case.

5.3 Detection limits for weak absorbers

Recent studies have shown that by exploiting weak absorption lines observed in the IASI spectra, total columns can also be retrieved for less abundant gases such as sulfur dioxide, ammonia, methanol and formic acid (Clarisse et al., 2011). This is especially the case when special events happen, such as volcanic eruption, large fires and pollution events, for which a series of molecules can be retrieved simultaneously (e.g. Coheur et al., 2009, R'Honi et al., 2013). The associated errors are rather large as the signal barely exceeds the noise level.

In the following, simulations were performed in order to determine the potential improvement in terms of detection limits when increasing the radiometric and spectral resolution performance. Different atmospheric situations were investigated. The figures provided here are for the tropical case situation, for which the impact of water vapour lines interferences is the strongest.

5.3.1 Sulfur dioxide (SO_2)

SO_2 absorbs thermal infrared radiation in the ν_1 band around 1150 cm^{-1}, the ν_3 band around 1350 cm^{-1} and the $\nu_1 + \nu_3$ band around 2500 cm^{-1} (Clarisse et al., 2012). The ν_3 band is the most prominent but lies in a range where strong absorptions by methane and water vapour occur, which makes it difficult to accurately retrieve tropospheric SO_2 concentrations.

Figure 15 illustrates the gain in the detection, as a function of altitude, obtained when using the ν_1, the ν_3, and the $\nu_1 + \nu_3$ bands. The simulations were performed as follows: different brightness temperature spectra were generated by increasing the SO_2 volume mixing ratio at different altitudes, in order to access the sensitivity at each altitude for different concentrations. The impact is checked using different channels, which were found to be the more intense in each spectral band: for ν_1, around 1163.2 and 1166.7 cm^{-1}; for ν_3, around 1348.3, 1352.6,1370.5, and 1371.50 cm^{-1} (the latter is as in the study of Clarisse et al., 2012) and for $\nu_1 + \nu_3$, 2498.8, and 2511.25 cm^{-1}. The improvement is quantified as the ratio between the detection limit for each scenario and the IRS1a-IASI one. It ranges between 25 % for IRS2a (blue line) and 80 % for IRS2c (red line) depending on the absorption band and scenario, provided the altitude is above 5 km. Between 0 and 3 km the improvement is limited to the ν_1 band which lies in an atmospheric window, whereas in the ν_3 band the strong interferences with water vapour is hiding the SO_2 signature close to the surface. As expected, due to the weak atmospheric signature of SO_2, a larger gain is obtained for a reduced noise, and the improvement of the spectral resolution has a smaller impact. It is worth noting that the simulations were performed with an unfavorable thermal contrast (difference between the surface temperature and the atmospheric temperature at the first altitude level) value of zero.

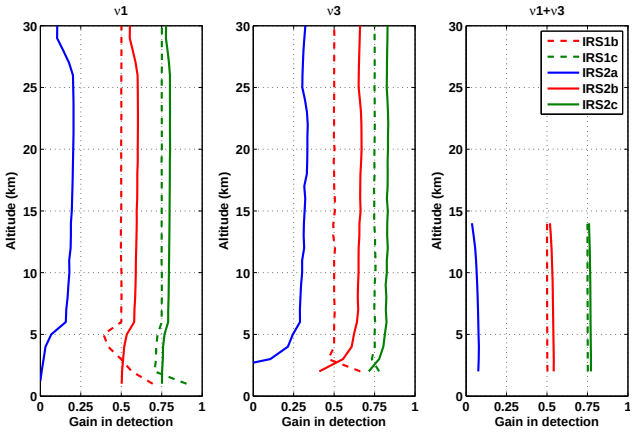

Figure 15. Impact study on the detection limit for SO_2. The plot represents the relative difference ratio between the detection limit of each scenario and the IRS1a-IASI scenario, as a function of altitude, for a case representative of a tropical atmospheric situation, when using the ν_1 band (left), ν_3 band (middle) and the $\nu_1 + \nu_3$ band (right). Note that the sensitivity of the latter band is limited to under 15 km.

Larger values of thermal contrast will enhance the detection level, especially at the surface.

5.3.2 Ammonia

Ammonia is emitted at surface level and rapidly destroyed. It absorbs infrared radiation in the ν_2 vibrational band with a clear signature around 950 cm^{-1} and lines covering the full region 750–1200 cm^{-1}. Although daily observations are possible close to the largest emission sources, the absorption signature in the IASI spectra is often of the same magnitude as the noise. In previous publications (e.g. Clarisse et al., 2009), measurements were averaged over long time periods in order to increase the signal-to-noise ratio. Here the simulations were performed using the intense NH_3 feature around 967.3 cm^{-1} (see Clarisse et al., 2010) and using increments of concentration for NH_3, with the different scenario configurations. As can be seen from Fig. 16, a factor of 2 improvement in the spectral resolution leads to a 25 % gain in detection sensitivity at the surface level for scenario IRS2a (blue line), whereas a factor of 2 improvement in the noise specifications leads to an improvement of 50 %. This is because 'ammonia has a broad absorption feature around 967.3 cm^{-1}, so the impact of spectral resolution is limited. As for SO_2, the estimation of the detection limit has been made with a thermal contrast equal to zero. Large positive or negative thermal contrasts will improve the conditions of NH_3 detection at near-surface level (see Clarisse et al., 2010) and increase, given the improvement in spectral resolution, the gain of sensitivity of IASI-NG in comparison to IASI for boundary layer NH_3.

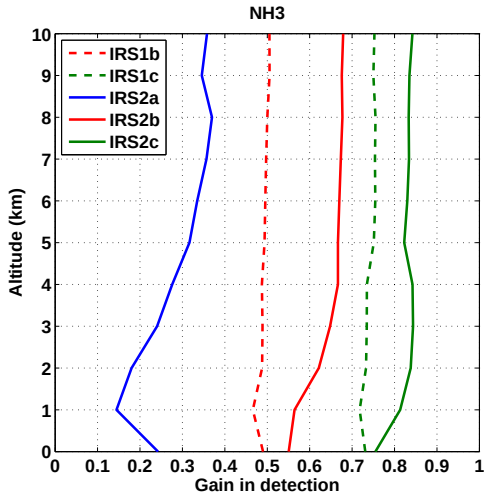

Figure 16. Impact study on the detection limit for NH_3. The plot represents the relative difference ratio between the detection limit of each scenario and the IRS1a-IASI scenario, as a function of altitude, for a case representative of a tropical atmospheric situation.

6 Summary and conclusion

The design of any satellite mission dedicated to atmospheric and surface remote sensing is a long-term process, which includes the definition of an instrumental concept that can fulfil a list of scientific requirements (Clerbaux and Crevoisier, 2013). Here we report on the detailed studies undertaken in the framework of the preparation of the EPS-SG payload, and we focus on the thermal infrared sounder IASI-NG, currently designed by CNES, that will provide information for the weather forecast, atmospheric composition and climate communities. The discussion is based on the IASI heritage and the investigated scenarios include combinations of improved spectral resolution (by a factor of 2) and improved radiometric performances (by factors of 2 to 4). These scenarios are used in radiative transfer simulations and retrieval procedures in order to investigate the impact on both accuracy and vertical information for various thermodynamic variables (temperature and water vapour profiles), climate variables (spectral emissivity, CO_2 and CH_4) and chemical tracers (CO and ozone). The detection limit for weak absorbers (SO_2 and ammonia) is also investigated.

The analysis of the retrieval performances shows that improving both the spectral resolution and radiometric noise leads to improvement of vertical resolution, accuracy and detection threshold for atmospheric and surface components. However, the specific impact and importance of both improvements depends on the retrieved variable. On the one hand, increasing the spectral resolution particularly matters when absorption lines of various gases located in the same spectral range interfere with each other (e.g. H_2O for the retrieval of CO and CH_4). Reducing the interferences thus leads to better accuracy. A higher spectral resolution also induces a better vertical resolution thanks to thinner weighting functions and Jacobians (e.g. temperature, CO). On the other hand, reducing the noise particularly matters for variables for which typical variations of brightness temperatures are of the level or much lower than the radiometric noise (CO_2, emissivity, and weak absorbers such as SO_2 and NH_3). Improving the radiometric noise thus yields improved signal to noise ratio, and translates into more accuracy for the retrieved variables, and more sensitivity lower in the atmosphere (e.g. T, H_2O, O_3). It should also lead to the detection of new "unexpected" species currently hidden in the noise, especially in large pollution plumes. Finally, at the moment the shortwave part of the spectrum covered by IASI is not well exploited because of noise issues. This study demonstrates that the noise reduction envisaged for IASI-NG is important as channels in this spectral range present sensitivity to the lower part of the troposphere. Being also able to use them in retrieval or assimilation procedures will thus further improve vertical resolution and accuracy in that part of the atmosphere.

It is worth noting that the impact of decreasing the size of the field-of-view (FOV) as compared to IASI has not been studied here, following the specifications of IASI-NG defined by CNES and EUMETSAT (EUMETSAT, 2010). On the one hand, reducing the size of the FOV would make it possible to obtain more clear-sky situations, and thus potentially increase the number of observations used in NWP systems or in retrievals. It would also help in obtaining more homogeneous scenes. On the other hand, reducing the pixel size would increase the radiometric noise and thus degrade the improvement in both precision and vertical coverage that is foreseen with the scenarios studied here. It would also impact the homogeneity of long-term climatologies of several ECVs derived from previous IR sounders (TOVS, ATOVS, AIRS) which had the same size of FOV as IASI and IASI-NG. A combined study focusing on determining the impact of a reduction of the FOV size, along with associated change in spectral and radiometric characteristics, on the capability to retrieve atmospheric and surface variables remains to be performed.

This study has focused on the retrieval of each variable in a stand-alone approach, without taking into account the improvement brought simultaneously to every variable. This will require performing Observing System Simulation Experiments (OSSEs) (e.g. Edwards et al., 2009). In particular, the expected improvement on the characterization of thermodynamic profiles and surface properties (spectral emissivity and surface temperature) will positively impact the retrievals of other atmospheric variables (e.g. trace gases) which usually require a good knowledge of the thermodynamic state of the atmosphere and the surface. It will also benefit several applications based on the retrieved level-2 products. For instance, the detection of ice supersaturation (relative humidity with respect to ice (RHice) exceeding 100 %), which is a necessary condition for ice nucleation as well as for the persistence of condensation trails induced by air traffic (Lamquin et

al., 2012), will be improved thanks to the expected improvement of the retrieval of water vapour, as shown by a preliminary comparison between AIRS and IASI (Stubenrauch et al., 2013).

With the planned launch of three successive instruments onboard the Metop-SG satellite suites (planned to be launched in 2020, 2027 and 2034), the IASI-NG mission will extend the 15-years IASI series by 20 years and, thanks to enhancements in both spectral resolution and radiometric noise, and will give access to better resolved and more accurate atmospheric and surface variables. IASI-NG will thus strongly benefit the numerical weather prediction, chemistry and climate communities now connected through the European GMES/Copernicus initiative.

The Supplement related to this article is available online at doi:10.5194/amt-7-4367-2014-supplement.

Acknowledgements. This research has received funding from CNES. The authors particularly wish to thank the IASI-NG Project Team at CNES and the EPS-SG team at EUMETSAT for fruitful discussions. Calculations were performed at IDRIS, the computer centre of CNRS, and at ClimServ, the data and computer centre of IPSL.

Edited by: A. Lambert

The publication of this article is financed by CNRS-INSU.

References

Boynard, A., Clerbaux, C., Coheur, P.-F., Hurtmans, D., Turquety, S., George, M., Hadji-Lazaro, J., Keim, C., and Meyer-Arnek, J.: Measurements of total and tropospheric ozone from IASI: comparison with correlative satellite, ground-based and ozonesonde observations, Atmos. Chem. Phys., 9, 6255–6271, doi:10.5194/acp-9-6255-2009, 2009.

Capelle, V., Chédin, A., Péquignot, E., Schluessel, P., Newman, S. M., and Scott, N. A.: Infrared continental surface emissivity spectra and skin temperature retrieved from IASI observations over the tropics, J. Appl. Meteorol. Clim., 51, 1164–1179, doi:10.1175/JAMC-D-11-0145.1, 2012.

Chalon, G., Cayla, F., and Diebel, D.: IASI: An Advanced Sounder for Operational Meteorology, Proceedings of the 52nd Congress of IAF, Toulouse France, October 2001, 2001.

Chédin, A., Scott, N. A., Wahiche, C., and Moulinier, P.: The improved initialisation inversion method: A high resolution physical method for temperature retrievals from satellites of the TIROS-N series, J. Clim. Appl. Meteorol., 24, 128–143, 1985.

Chédin, A., Saunders, R., Hollingsworth, A., Scott, N. A., Matricardi, M., Etcheto, J., Clerbaux, C., Armante, R., and Crevoisier, C.: The feasibility of monitoring CO_2 from high-resolution infrared sounders, J. Geophys. Res., 108, 4064, doi:10.1029/2001JD001443, 2003.

Chevallier, F., Chéruy, F., Scott, N. A., and Chédin, A.: A neural network approach for a fast and accurate computation of a long-wave radiative budget, J. Appl. Meteorol., 37, 1385–1397, 1998.

Clarisse, L., Clerbaux, C., Dentener, F., Hurtmans, D., and Coheur, P.-F.: Global ammonia distribution derived from infrared satellite observations, Nat. Geosci., 2, 479–483, doi:10.1038/ngeo551, 2009.

Clarisse, L., Hurtmans, D., Prata, A. J., Karagulian, F., Clerbaux, C., De Mazière, M., and Coheur, P.-F.: Retrieving radius, concentration, optical depth, and mass of different types of aerosols from high-resolution infrared nadir spectra, Appl. Optics, 49, 3713–3722, 2010.

Clarisse, L., R'Honi, Y., Coheur, P.-F., Hurtmans, D., and Clerbaux, C.: Thermal infrared nadir observations of 24 atmospheric gases, Geophys. Res. Lett., 38, L10802, doi:10.1029/2011GL047271, 2011.

Clarisse, L., Hurtmans, D., Clerbaux, C., Hadji-Lazaro, J., Ngadi, Y., and Coheur, P.-F.: Retrieval of sulphur dioxide from the infrared atmospheric sounding interferometer (IASI), Atmos. Meas. Tech., 5, 581–594, doi:10.5194/amt-5-581-2012, 2012.

Clerbaux, C., Boynard, A., Clarisse, L., George, M., Hadji-Lazaro, J., Herbin, H., Hurtmans, D., Pommier, M., Razavi, A., Turquety, S., Wespes, C., and Coheur, P.-F.: Monitoring of atmospheric composition using the thermal infrared IASI/MetOp sounder, Atmos. Chem. Phys., 9, 6041–6054, doi:10.5194/acp-9-6041-2009, 2009.

Clerbaux, C. and Crevoisier, C.: New Directions: Infrared remote sensing of the troposphere from satellite: Less, but better, Atmos. Environ., 72, 24–26, doi:10.1016/j.atmosenv.2013.01.057, 2013.

Coheur, P.-F., Clarisse, L., Turquety, S., Hurtmans, D., and Clerbaux, C.: IASI measurements of reactive trace species in biomass burning plumes, Atmos. Chem. Phys., 9, 5655–5667, doi:10.5194/acp-9-5655-2009, 2009.

Collard, A. D. and McNally, A. P., The assimilation of Infrared Atmospheric Sounding Interferometer radiances at ECMWF, Q. J. Roy. Meteor. Soc., 135, 1044–1058, 2009.

Crevoisier, C., Chédin, A., and Scott, N. A.: AIRS channel selection for CO_2 and other trace-gas retrievals, Q. J. Roy. Meteor. Soc., 129, 2719–2740, 2003.

Crevoisier, C., Chédin, A., Matsueda, H., Machida, T., Armante, R., and Scott, N. A.: First year of upper tropospheric integrated content of CO_2 from IASI hyperspectral infrared observations, Atmos. Chem. Phys., 9, 4797–4810, doi:10.5194/acp-9-4797-2009, 2009a.

Crevoisier, C., Nobileau, D., Fiore, A. M., Armante, R., Chédin, A., and Scott, N. A.: Tropospheric methane in the tropics – first year from IASI hyperspectral infrared observations, Atmos. Chem. Phys., 9, 6337–6350, doi:10.5194/acp-9-6337-2009, 2009b.

Crevoisier, C., Nobileau, D., Armante, R., Crépeau, L., Machida, T., Sawa, Y., Matsueda, H., Schuck, T., Thonat, T., Pernin, J., Scott, N. A., and Chédin, A.: The 2007–2011 evolution of tropical methane in the mid-troposphere as seen from space by MetOp-A/IASI, Atmos. Chem. Phys., 13, 4279–4289, doi:10.5194/acp-13-4279-2013, 2013.

De Wachter, E., Barret, B., Le Flochmoën, E., Pavelin, E., Matricardi, M., Clerbaux, C., Hadji-Lazaro, J., George, M., Hurtmans, D., Coheur, P.-F., Nedelec, P., and Cammas, J. P.: Retrieval of MetOp-A/IASI CO profiles and validation with MOZAIC data, Atmos. Meas. Tech., 5, 2843–2857, doi:10.5194/amt-5-2843-2012, 2012.

Duflot, V., Hurtmans, D., Clarisse, L., R'Honi, Y., Vigouroux, C., De Mazière, M., Mahieu, E., Servais, C., Clerbaux, C., and Coheur, P.-F.: Measurements of hydrogen cyanide (HCN) and acetylene (C_2H_2) from the Infrared Atmospheric Sounding Interferometer (IASI), Atmos. Meas. Tech., 6, 917–925, doi:10.5194/amt-6-917-2013, 2013.

Dufour, G., Eremenko, M., Griesfeller, A., Barret, B., LeFlochmoën, E., Clerbaux, C., Hadji-Lazaro, J., Coheur, P.-F., and Hurtmans, D.: Validation of three different scientific ozone products retrieved from IASI spectra using ozonesondes, Atmos. Meas. Tech., 5, 611–630, doi:10.5194/amt-5-611-2012, 2012.

Edwards, D. P., Arellano, A. F., and Deeter, M. N.: A satellite observation system simulation experiment for carbon monoxide in the lowermost troposphere, J. Geophys. Res., 114, D14304, doi:10.1029/2008JD011375, 2009.

Eremenko, M., Dufour, G., Foret, G., Keim, C., Orphal, J., Beekmann, M., Bergametti, G., and Flaud, J.-M.: Tropospheric ozone distributions over Europe during the heat wave in July 2007 observed from infrared nadir spectra recorded by IASI, Geophys. Res. Lett., 35, L18805, doi:10.1029/2008GL034803, 2008.

EUMETSAT, Post-EPS Mission Requirements Document, EUM/PEPS/REQ/06/0043, v3A, http://aramis.obspm.fr/~gdr/GDR/Documents_files/Post-EPS-2008.pdf (last access: 9 December 2013), 2010.

Gambacorta, A., Barnet, C., Wolf, W., King, T., Maddy, E., Strow, L., Xiong, X., Nalli, N., and Goldberg, M.: An Experiment Using High Spectral Resolution CrIS Measurements for Atmospheric Trace Gases: Carbon Monoxide Retrieval Impact Study, IEEE Geosci. Remote S., 11, 1639–1643, 2014.

GCOS-107, Systematic observation requirements for satellite-based products for climate, Supplemental details to the satellite-based component of the "Implementation Plan for the Global Observing System for Climate in Support of the UNFCCC", September 2006, WMO/TD No. 1338, WMO – World Meteorological Organization, Intergovernmental Oceanographic Commission, United Nations Environment Programme, and International Council for Science, available at: http://www.wmo.int/pages/prog/gcos/Publications/gcos-107.pdf (last access: 9 December 2013), 2006.

GCOS-154, Systematic observation requirements for satellite-based products for climate – 2011 update, December 2011, , WMO – World Meteorological Organization, Intergovernmental Oceanographic Commission, United Nations Environment Programme, and International Council for Science, available at: http://www.wmo.int/pages/prog/gcos/Publications/gcos-154.pdf(last access: 9 December 2013), 2011.

George, M., Clerbaux, C., Hurtmans, D., Turquety, S., Coheur, P.-F., Pommier, M., Hadji-Lazaro, J., Edwards, D. P., Worden, H., Luo, M., Rinsland, C., and McMillan, W.: Carbon monoxide distributions from the IASI/METOP mission: evaluation with other space-borne remote sensors, Atmos. Chem. Phys., 9, 83170–8330, doi:10.5194/acp-9-8317-2009, 2009.

Guidard, V., Fourrié, N., Brousseau, P., and Rabier, F.: Impact of IASI assimilation at global and convective scales and challenges for the assimilation of cloudy scenes, Q. J. Roy. Meteor. Soc., 137, 1975–1987, doi:10.1002/qj.928, 2011.

Herbin, H., Hurtmans, D., Turquety, S., Wespes, C., Barret, B., Hadji-Lazaro, J., Clerbaux, C., and Coheur, P.-F.: Global distributions of water vapour isotopologues retrieved from IMG/ADEOS data, Atmos. Chem. Phys., 7, 3957–3968, doi:10.5194/acp-7-3957-2007, 2007.

Herbin, H., Hurtmans, D., Clerbaux, C., Clarisse, L., and Coheur, P.-F.: $H_2^{16}O$ and HDO measurements with IASI/MetOp, Atmos. Chem. Phys., 9, 9433–9447, doi:10.5194/acp-9-9433-2009, 2009.

Hólm, E., Andersson, E., Beljaars, A., Lopez, P., Mahfouf, J.-F., Simmons A. J., and Thépaut, J.-N.: Assimilation and modelling of the hydrological cycle: ECMWF's Status and Plan, ECMWF Tech. Memo., 383, ECMWF, 2002.

Hilton, F., Armante, R., August, T., Barnet, C., Bouchard, A., Camy-Peyret, C., Capelle, V., Clarisse, L., Clerbaux, C., Coheur, P.-F., Collard, A., Crevoisier, C., Dufour, G., and Edwards, D. Faijan, F., Fourrié, N., Gambacorta, A., Goldberg, M., Guidard, V., Hurtmans, D., Illingworth, S., Jacquinet-Husson, N., Kerzenmacher, T., Klaes, D., Lavanant, L., Masiello, G., Matricardi, M., McNally, A., Newman, S., Pavelin, E., Payan, S., Péquignot, E., Peyridieu, S., Phulpin, T., Remedios, J., Schlüssel, P., Serio, C., Strow, L., Stubenrauch, C., Taylor, J., Tobin, D., Wolf, W., and Zhou, D., Hyperspectral Earth Observation from IASI: Five Years of Accomplishments, B. Am. Meteorol. Soc., 93, 347–370, doi:10.1175/BAMS-D-11-00027.1, 2012.

Hurtmans, D., Coheur, P.-F., Wespes, C., Clarisse, L., Scharf, O., Clerbaux, C., Hadji-Lazaro, J., George, M., and Turquety, S.: FORLI radiative transfer and retrieval code for IASI, J. Quant. Spectrosc. Ra., 113, 1391–1408, 2012.

Jacquinet-Husson, N., Crepeau, L., Armante, R., Boutammine, C., Chédin, A., Scott, N. A., Crevoisier, C., Capelle, V., Boone, C., Poulet-Crovisier, N., Barbe, A., Campargue, A., Chris Benner, D., Benilan, Y., Bézard, B., Boudon, V., Brown, L. R., Coudert, L. H., Coustenis, A., Dana, V., Devi, V. M., Fally, S., Fayt, A., Flaud, J.-M., Goldman, A., Herman, M., Harrio, G. J., Jacquemart, D., Jolly, A., Kleiner, I., Kleinböhl, A., Kwabia-Tchana, F., Lavrentieva, N., Lacome, N., Li-Hong, X., Lyulin, O. M., Mandin, J.-Y., Maki, A., Mikhailenko, S., Miller, C. E., Mishina, T., Moazzen-Ahmadi, N., Müller, H. S. P., Nikitin, A., Orphal, J., Perevalov, V., Perrin, A., Petkie, D. T., Predoi-Cross, A., Rinsland, C. P., Remedios, J. J., Rotger, M., Smith, M. A. H., Sung, K., Tashkun, S., Tennyson, J., Toth, R. A., Vandaele, A.-C., and Vander Auwera, J.: The 2009 edition of the GEISA spectroscopic database, J. Quant. Spectrosc. Ra., 112, 2395–2445, doi:10.1016/j.jqsrt.2011.06.004, 2011.

Kerzenmacher, T., Dils, B., Kumps, N., Blumenstock, T., Clerbaux, C., Coheur, P.-F., Demoulin, P., García, O., George, M., Griffith, D. W. T., Hase, F., Hadji-Lazaro, J., Hurtmans, D., Jones, N., Mahieu, E., Notholt, J., Paton-Walsh, C., Raffalski, U., Ridder, T., Schneider, M., Servais, C., and De Mazière, M.: Validation of IASI FORLI carbon monoxide retrievals using FTIR data from NDACC, Atmos. Meas. Tech., 5, 2751–2761, doi:10.5194/amt-5-2751-2012, 2012.

Klüser, L., Kleiber, P., Holzer-Popp, T., and Grassia, V. H., Desert dust observation from space – Application of measured min-

eral component infrared extinction spectra, Atmos. Environ., 54, 419–427, doi:10.1016/j.atmosenv.2012.02.011, 2012.

Kulawik, S. S., Osterman, G., Jones, D. B. A., and Bowman, K. W.: Calculation of altitude-dependent Tikhonov constraints for TES nadir retrievals, IEEE T. Geosci. Remote, 44, 1334–1342, 2006.

Kwon, E.-H., Sohn, B. J., Smith, W. L., and Li, J.: Validating IASI Temperature and Moisture Sounding Retrievals over East Asia Using Radiosonde Observations, J. Atmos. Ocean. Tech., 29, 1250–1262, doi:10.1175/JTECH-D-11-00078.1, 2012.

Lacour, J.-L., Risi, C., Clarisse, L., Bony, S., Hurtmans, D., Clerbaux, C., and Coheur, P.-F.: Mid-tropospheric δD observations from IASI/MetOp at high spatial and temporal resolution, Atmos. Chem. Phys., 12, 10817–10832, doi:10.5194/acp-12-10817-2012, 2012.

Lamquin, N., Stubenrauch, C. J., Gierens, K., Burkhardt, U., and Smit, H.: A global climatology of upper-tropospheric ice supersaturation occurrence inferred from the Atmospheric Infrared Sounder calibrated by MOZAIC, Atmos. Chem. Phys., 12, 381–405, doi:10.5194/acp-12-381-2012, 2012.

Lezeaux, O., Pierangelo, C., Scott, N. A., Camy-Peyret, C., Cassé, V., Klonecki, A., Prunet, P., Payan, S., Armante, R., Capelle, V., and Phulpin, T.: Temperature sounding from IASI using N_2O channels: Theoretical study and validation with JAIVEx observations, 2nd IASI International Conference, Annecy, France, 25–29 January, 2010.

Niro, F., Boulet, C., and Hartmann, J.-M.: Spectra calculations in central and wing regions of CO_2 IR bands between 10 and 20 µm. I: model and laboratory measurements, J. Quant. Spectrosc. Ra., 88, 4, 483–498, doi:10.1016/j.jqsrt.2004.04.003, 2004a.

Niro, F., von Clarmann, T., Jucks, K., and Hartmann, J.-M.: Spectra calculations in central and wing regions of CO_2 IR bands between 10 and 20 µm. III: atmospheric emission spectra, J. Quant. Spectrosc. Ra., 90, 61–76, doi:10.1016/j.jqsrt.2004.04.005, 2004b.

Péquignot, E., Chédin, A., and Scott, N. A.: Infrared continental surface emissivity spectra retrieved from AIRS hyperspectral sensor, J. Appl. Meteorol. Clim., 47, 1619–1633, 2008.

Peyridieu, S., Chédin, A., Capelle, V., Tsamalis, C., Pierangelo, C., Armante, R., Crevoisier, C., Crépeau, L., Siméon, M., Ducos, F., and Scott, N. A.: Characterisation of dust aerosols in the infrared from IASI and comparison with PARASOL, MODIS, MISR, CALIOP, and AERONET observations, Atmos. Chem. Phys., 13, 6065–6082, doi:10.5194/acp-13-6065-2013, 2013.

Pougatchev, N., August, T., Calbet, X., Hultberg, T., Oduleye, O., Schlüssel, P., Stiller, B., Germain, K. St., and Bingham, G.: IASI temperature and water vapor retrievals – error assessment and validation, Atmos. Chem. Phys., 9, 6453–6458, doi:10.5194/acp-9-6453-2009, 2009.

Prunet, P., Thépaut, J. N., and Cassé, V.: The information content of clear-sky IASI radiances and their potential for numerical weather prediction, Q. J. Roy. Meteor. Soc., 124, 211–242, 1998.

Razavi, A., Karagulian, F., Clarisse, L., Hurtmans, D., Coheur, P. F., Clerbaux, C., Müller, J. F., and Stavrakou, T.: Global distributions of methanol and formic acid retrieved for the first time from the IASI/MetOp thermal infrared sounder, Atmos. Chem. Phys., 11, 857–872, doi:10.5194/acp-11-857-2011, 2011.

R'Honi, Y., Clarisse, L., Clerbaux, C., Hurtmans, D., Duflot, V., Turquety, S., Ngadi, Y., and Coheur, P.-F.: Exceptional emissions of NH_3 and HCOOH in the 2010 Russian wildfires, Atmos. Chem. Phys., 13, 4171–4181, doi:10.5194/acp-13-4171-2013, 2013.

Rodgers, C. D.: Information content and optimization of high spectral resolution measurements, Optical Spectroscopic Techniques and Instrumentation for Atmospheric and Space Research II, SPIE, 2830, 136–147, 1996.

Rodgers, C. D.: Inverse Methods for Atmospheric Sounding: Theory and Practice, World Sci., Hackensack, N. J., 2000.

Rumelhart, D. E., Hinton, G. E., and Williams, R. J.: Learning internal representations by error propagation, in: Parallel Distributed Processing: Explorations in the Macrostructure of Cognition, vol. 1, edited by: Rumelhart, D. E. and McClelland, J. L., MIT Press, Cambridge, Mass, 318–362, 1986.

Scott, N. A. and Chédin, A.: A fast line-by-line method for atmospheric absorption computations: The Automatized Atmospheric Absorption Atlas, J. Appl. Meteorol., 20, 802–812, 1981.

Sellitto, P., Dufour, G., Eremenko, M., Cuesta, J., Dauphin, P., Forêt, G., Gaubert, B., Beekmann, M., Peuch, V.-H., and Flaud, J.-M.: Analysis of the potential of one possible instrumental configuration of the next generation of IASI instruments to monitor lower tropospheric ozone, Atmos. Meas. Tech., 6, 621–635, doi:10.5194/amt-6-621-2013, 2013.

Stubenrauch, C., Feofilov, A., Armante, R., and Guignard, A.: Cloud properties & bulk microphysical properties of semi-transparent cirrus from AIRS & IASI, Third IASI International Conference, Hyères, 4–8 February 2013.

Thonat, T., Crevoisier, C., Scott, N. A., Chédin, A., Schuck, T., Armante, R., and Crépeau, L.: Retrieval of tropospheric CO column from hyperspectral infrared sounders – application to four years of Aqua/AIRS and MetOp-A/IASI, Atmos. Meas. Tech., 5, 2413–2429, doi:10.5194/amt-5-2413-2012, 2012.

Worden, J., Bowman, K., Noone, D., Beer, R., Clough, S., Eldering, A., Fisher, B., Goldman, A., Gunson, M., Herman, R., Kulawik, S., Lampel, M., Luo, M., Osterman, G., Rinsland, C., Rodgers, C., Sander, S., Shephard, M., and Worden, H.: Tropospheric Emission Spectrometer observations of the tropospheric HDO/H_2O ratio: Estimation approach and characterization, 25 August, J. Geophys. Res., 111, D16309, doi:10.1029/2005JD006606, 2006.

Worden, H. M., Logan, J. A., Worden, J. R., Beer, R., Bowman, K., Clough, S. A., Eldering, A., Fisher, B. M., Gunson, M. R., Herman, R. L., Kulawik, S. S., Lampel, M. C., Luo, M., Megretskaia, I. A., Osterman, G. B., and Shephard, M. W.: Comparisons of Tropospheric Emission Spectrometer (TES) ozone profiles to ozonesondes: Methods and initial results, J. Geophys. Res., 112, D03309, doi:10.1029/2006JD007258, 2007.

Zakharov, V. I., Imasu, R., Gribanov, K. G., Hoffmann, G., and Jouzel, J.: Latitudinal distribution of the deuterium to hydrogen ratio in the atmospheric water vapour retrieved from IMG/ADEOS data, Geophys. Res. Lett., 31, L12104, doi:10.1029/2004GL019433, 2004.

Zhou, D. K., Larar, A. M., Liu, X., Smith, W. L., Strow, L. L., Yang, P., Schlüssel, P., and Calbet, X., Global land surface emissivity retrieved from satellite ultraspectral IR measurements, IEEE T. Geosci. Remote, 49, 1277–1290, doi:10.1109/TGRS.2010.2051036, 2011.